Effects of Corona Discharges on Silicone Rubber Samples under Severe Environmental Conditions

by

Mohammad Ali Hakami

A thesis
presented to the University of Waterloo
in fulfillment of the
thesis requirement for the degree of
Master of Applied Science
in
Electrical and Computer Engineering

Waterloo, Ontario, Canada, 2020

AUTHOR'S DECLARATION

I hereby declare that I am the sole author of this thesis. This is a true copy of the thesis, including any required final revisions, as accepted by my examiners.

I understand that my thesis may be made electronically available to the public.

Abstract

Silicone rubber (SiR) material has been utilized as a replacement to ceramic insulators. The impetus for increasing SiR applications in outdoor insulators is its unique hydrophobicity. However, SiR insulators are subjected to different stresses that may lead to their aging, hence the loss of their hydrophobic properties. The aging of SiR insulators is dependent on several factors. Some of these factors are related to weather, while others associated with system conditions, including electrical discharges generated from corona and/or dry band arcing. These factors also may possess synergistic impact, which can aggravate the aging process.

Studying the SiR resistance to corona can be considered of great interest because the corona is one of the critical aging factors affecting the SiR insulators. Moreover, severe environmental conditions like ultraviolet (UV) radiation and high humidity can accelerate the aging process caused by corona. Hence, extensive research has been conducted to understand the performance of silicone rubber material exposed to corona discharges under varied weather conditions. However, the literature to analyze the synergetic effect of corona and various weather conditions on the aging of silicone rubber materials is still insufficient. This motivates to investigate the impact of corona along with other weather conditions on the aging of SiR material.

In the present research, experiments are conducted by generating corona discharges using a high AC voltage of 10 kV applied to sharp needle electrodes on the surface of SiR samples for 24 hours. The gap distance between the surface of samples and the tip of the needle was set at 6 mm. The experiment is performed inside a testing chamber where both the humidity level and UV radiation can be controlled. The UV radiation with 1 mW/cm^2 intensity is generated from UVA-340 lamps. The humidity level inside the test chamber is increased through creating mist from deionized water using an ultrasonic humidifier. Three humidity levels are considered, i.e. high humidity (80 to 90%), medium humidity (65 to 75%), and low humidity (30 to 40%).

At each testing conditions, three silicone samples are tested simultaneously. After the experiment of this study, the silicone rubber degradation is assessed using the static contact angle measurements. The measurement is taken for 100 hours to quantify the hydrophobicity loss and recovery. It has been found that considerable hydrophobicity loss in all SiR samples is originated by corona aging test. Furthermore, the outcomes show that both the UV radiation and humidity possess considerable effect on the

hydrophobicity loss and recovery. For further understanding, the scanning electron microscopy (SEM) and energy-dispersive X-ray spectroscopy (EDX) have been used to investigate the intensity of surface damage. Results of SEM analysis show signs of aging in the SiR samples such as craters and cracks. Based on EDX findings, it has been found that considerable reduction in aluminum trihydrate (ATH) content, which plays important role in erosion and tracking resistance, on the SiR samples surface. Overall, it has been shown that samples tested at both high humidity and UV radiation conditions suffered from the worst corona effects, whereas the low humidity with no UV condition has the least corona impacts.

Acknowledgements

In the Name of Allah, the Most Gracious, the Most Merciful, all the praises and thanks be to Allah, the Lord of the worlds, for granting me success in my entire life and for gaining me strength and knowledge to complete this study. Prayers and peace be upon our Prophet Muhammad who said that the best of people is the most beneficial to people. This saying was one of the main motivations for my study in order to serve people by my knowledge.

I would like to express my sincere appreciation to supervisors, Prof. Shesha Jayaram and Prof. Ayman El-Hag, who were continual sources of inspiration and encouragement to make the way to fulfillment of the degree of Masters of Applied Science easy for me. I wish to thank them for their unforgettable efforts, appreciable supports, and their valuable patience they have provided during supervising my research. I wish I would be always fulfilling the expectations.

I am highly indebted to Poly-Nova Technologies for their support by supplying silicone rubber material samples, for performing the corona aging test. I would like to express my thanks to my colleague Amin Gorji who lent me humidity sensor. I would like to thank Mohana Krishnan, manager of High Voltage Engineering Laboratory (HVEL), for his help. Special thanks are due to my other colleagues in HVEL, including Faisal Aldawsari, Khadija Khanum, Anurag Devadiga, and Ibrahim Marwan Jarrar, for their support as well as the moments we spent together. I would like to express my appreciation to all my friends in Waterloo and Saudi Arabia.

I acknowledge the financial support from King Saud University in the Kingdom of Saudi Arabia and from the Saudi Cultural Bureau in Canada. My gratitude goes to Prof. Kankar Bhattacharya and Prof. Ramadan El Shatshat for accepting to be the readers for my thesis and for their comments on my thesis.

I owe my deepest gratitude to my wife, Hadeel, for her love, encouragement, understanding, prayers, and patience resulting in overcoming many obstacles during my life, including graduate study. Special thanks go to my son, Ali, who fills my life with happiness and joy.

I would like to express my deep thanks to my siblings, Yasser, Mu'ath, Yusra, Dania, Do'aa, Khawla, Anas, and Abdulaziz, for their love, supports, and prayers. Do'aa, I am sorry I could not attend your wedding because I was so busy with my study in Canada.

My greatest thanks and gratitude are devoted to my parents, Ali and ebtisam, from whom I get my strength. Their wisdom, intelligence, love, encouragement, upbringing, sacrifice, prayers, and directions have played an important role in my whole life. Dad and Mom, it is impossible for me to fully express my gratitude for your efforts towards me.

Dedication

To my dear parents, my beloved wife, my charming son, my precious brothers and sisters, and my esteemed teachers and researchers.

Table of Contents

List of Figures

.

List of Tables

Chapter 1
Introduction

1.1 Preamble

Currently, the thriving advancement in power systems drives manufactures of high voltage apparatuses to produce components with enhanced performances, increased reliability, and longer lifetime. One of these essential components is outdoor insulators that holds the line conductors mechanically and electrically isolates them from the grounded tower. For preventing their failure, such insulators must possess suitable properties in order to meet the criteria in terms of electrical, mechanical, economic, and environmental conditions. Nonetheless, those properties are determined by several factors. One of these important factors is material of the outdoor insulators. Based on the material, the outdoor insulators can be either ceramic insulators or non-ceramic insulators. The former are made of either glass or porcelain, while the latter contain a housing of polymeric material which is primarily either ethylene propylene diene monomer (EPDM) elastomer, silicone rubber (SiR), or copolymers of SiR and EPDM.

Although the raw material of the ceramic insulators is less expensive, the properties of non-ceramic insulators outperform the ceramic insulators in respect of weight, flexibility, surface area, creepage distance, and performance under pollution conditions. Also, the excellent hydrophobicity is a feature specific to the non-ceramic insulators, especially the SiR [1,2]. Over the last several decades, immense data about service experience of non-ceramic insulators, i.e. polymeric insulators, used throughout the world is gathered by CIGRE community [3,4]. For example, a survey was performed by CIGRE for investigating the worldwide spread of polymeric insulators for voltage levels exceeding 69 kV. The results of such survey show that the SiR insulators are the most prevalent insulators utilized at the aforementioned voltage levels which is evident in Figure 1.1.

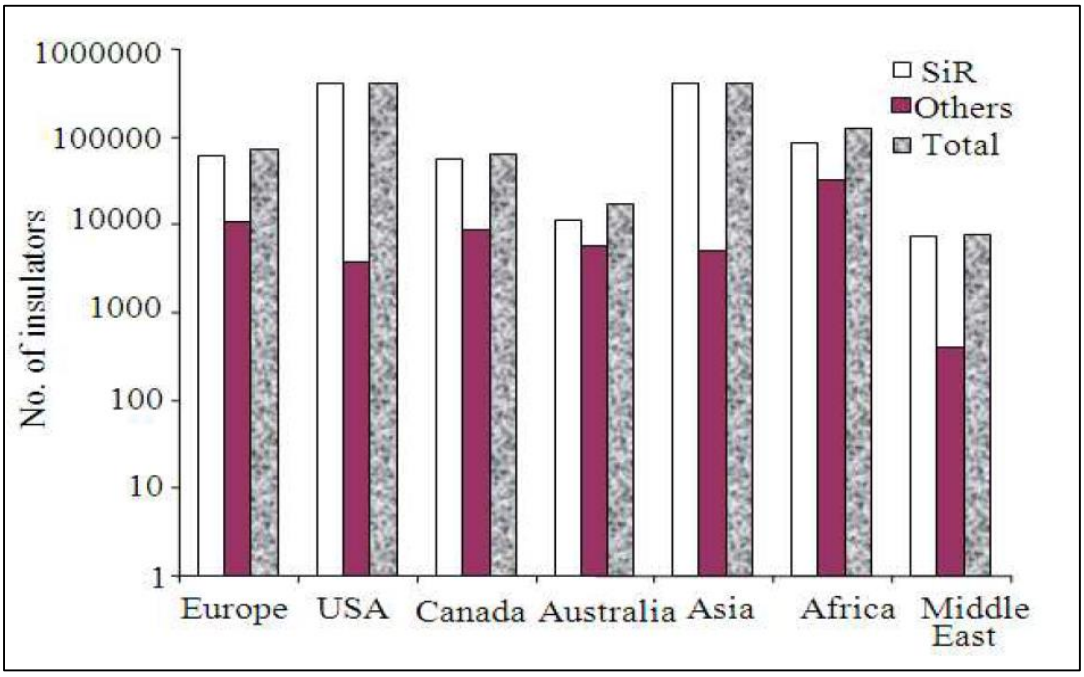

Figure 1.1. Polymeric insulators utilized in the world [3,4].

Despite the huge research and the wide experience related to non-ceramic insulators, a sufficient standard for their required properties used in high voltage application has not yet been provided. In addition, utilities as well as manufacturers demand material standards containing the physical properties of the SiR and other polymers used for outdoor insulation. Therefore, CIGRE Working Group D1.14 specified twelve desired physical properties of non-ceramic insulators. In addition, the relevant test techniques of those properties were provided when needed [5]. Eight of such properties are examined using standardized test methods. Those eight properties were arc resistance, chemical resistance, glass transition temperature, breakdown field strength, resistance to chemical and physical degradation, tear strength, resistance to tracking and erosion, and volume resistivity. The remaining four properties have no standardized tests. Such remaining properties included corona and ozone resistance, hydrophobicity, flame resistance, and resistance to weathering and UV. Among those properties, the resistance to corona is considered as being of great significance since the corona discharges are one of the aging factors affecting SiR insulators [12, 9].

1.2 Thesis Motivation

The importance of the resistance to corona has driven many researchers to investigate the performance of SiR insulators under corona discharges. These investigations could be either in laboratory or in the field. Because generation of continuous and controllable corona discharges is indispensable, the examination of SiR insulating materials exposed to corona discharges is performed predominantly in the laboratory. Silicone rubber material superior properties are deteriorated by both corona discharges and environmental stresses including humidity and ultraviolet (UV) radiation. Therefore, some studies concentrated on analyzing influences of corona discharges on SiR material under severe climatic conditions. Nevertheless, UV radiation as an aging factor was not fully considered in those studies although it is significant in some geographical areas. For instance, UV radiation level in Saudi Arabia is extremely critical [4]. Hitherto, no research, to the best of our knowledge, investigated the effects of corona and UV applied simultaneously on SiR insulation. Thus, filling the gap of this issue is the impetus for this thesis. Furthermore, the combined effects of other environmental conditions like humidity on SiR aging will be also investigated in our research.

1.3 Research Objectives

In this research, the work carried out at the University of Waterloo for investigating the impingement of the corona discharges on SiR materials used for high voltage outdoor insulators under stringent environmental conditions will be described. The main aim of this study comprises the following sequential steps: studying SiR insulators in terms of properties and aging factors, understanding physics of corona discharges, designing the required equipment for the test, proposing the test parameters, investigating the effects of the combination of corona, humidity, and/or UV on SiR aging, and finally evaluating the consequent changes in properties of the SiR specimens. The examined material properties consist of physical and chemical variations, and hydrophobicity behavior. The corresponding characterization techniques are scanning electron microscopy (SEM), energy-dispersive X-ray analysis (EDX) and static contact angle measurements. Ultimately, the results of the various test conditions will be compared.

1.4 Thesis Arrangement

The structure of this thesis is identified as listed below:

- Chapter 1, " Introduction", describes a preface for this work, succeeded by description of research motivation and major contributions.
- Chapter 2, " Background and Literature Review", provides a background of outdoor insulators with regard to their high voltage applications and types, followed by a review on silicone rubber insulation pertaining to the base material, categories, and properties. Moreover, aging process of the silicone rubber insulators in connection with electrical and environmental factors is described. Finally, a simple introduction to effects of corona discharges on silicone rubber insulators is presented, concluded by its literature review as regards the previous field and laboratory investigations.
- In Chapter 3, " Materials and Methods", the methodology for the experiments in connection with the artificial 24 h corona discharges aging test under diverse environmental conditions, i.e. humidity and ultraviolet radiation, is described in detail. Such description involves arrangement and procedure of the test and approaches utilized to characterize the SiR specimens.
- Chapter 4, " Results and Discussion", concentrates on reporting the experimental outcomes procured from the corona discharges aging tests through the methodology explained in Chapter 3. The findings of the varied climatic conditions are compared to ascertain that effect of both UV and/or humidity along with corona discharges on the aging of SiR material.
- Chapter 5, "Conclusions and Recommendations", presents conclusions deduced from this thesis and recommendations with regard to the future work in the area of the investigated topic.

Chapter 2
Background and Literature Review

2.1 Outdoor Insulators

The outdoor insulators are crucial components in overhead lines as they hold mechanically the line conductors and electrically isolate them from the grounded tower. Hence, outdoor insulators are subjected to both electrical and mechanical stresses. These stresses are classified into two types, steady state and transient stresses. Moreover, these insulators sustain other stresses that stem from the surrounding environmental conditions like UV, humidity and pollution. The UV radiations could change chemical bonds of some outdoor insulators' material due to polymer chain scission reactions. The pollution along with rain, fog, and/or moisture, may reduce the surface resistivity of the insulators. The temperature can increase the conductivity of the electrolyte on the insulators' surface.

Thus, an insulator must be designed cautiously to meet certain criteria so that it can withstand all types of stresses to avoid the possibility of any flashover or insulator failure. These criteria can be summarized as follows [1]:

(i) High dielectric strength in order that the insulator can withstand overvoltage even under harsh environmental conditions.
(ii) High mechanical strength to carry the conductor mechanical load under most severe weather situations.
(iii) High thermal conductivity.
(iv) High surface resistance.
(v) Smooth, concave downwards surface. This can assist in self-cleaning because of rain and wind.

To meet the aforementioned criteria, various Insulators are produced with different materials. These materials are categorized into ceramic and non-ceramic insulators.

2.2 Ceramic insulators

Ceramic insulators have been utilized in power transmission applications since 19^{th} century [6]. The outdoor ceramic insulators are made from either porcelain or glass materials. The porcelain is shaped from a homogeneous mix of wet plastic clay and glazed before firing in a kiln [1, 67]. By glazing, the surface can be kept relatively clean and dry. Dielectric strength of the porcelain can be significantly

reduced by embedded impurities. Hence, the porcelain must be entirely impervious. Also, it is important for the porcelain insulators to have sufficient creepage distance, especially under wet and contaminated conditions to minimize the flow of uncontrolled leakage current leading to flashover [1]. Figure 2.1 depicts the components of a cap and pin type porcelain insulator. These components are a glazed porcelain shell and galvanized steel cap and pin that are cemented together [7].

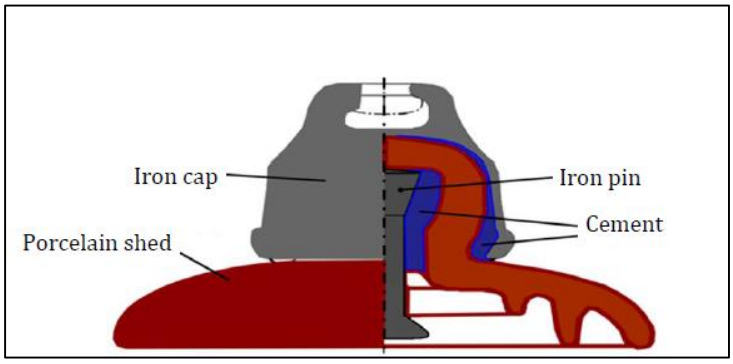

Figure 2.1. A cap and pin type porcelain insulator [7].

The other material used for the ceramic insulators is toughened glass, presented in Figure 2.2. The outer surface of the toughened glass is in compression while its interior is in tension. To produce this state, the glass insulator is rapidly cooled after shaping and the interior is cooled slowly. The advantages of the glass insulator are that it is cheaper than porcelain [1], and flaws can be easily detected due to its transparency. Nevertheless, glass is more affected by temperature variation than porcelain. In addition to this demerit, irregular shape of the glass insulator can lead to internal strain after cooling. As a result, the glass insulator possesses less reliability and prevalence than porcelain [1]. Moreover, porcelain is stronger mechanically and less affected by the temperature variations and leakage current. Hence, the porcelain is the most used material for outdoor insulators [1].

While ceramic insulators have been employed vastly owing to their high reliability and cost effectiveness, non-ceramic insulators have emerged and being utilized extensively [1].

Figure 2.2. A cap and pin glass insulator [8].

2.3 Non-ceramic insulators

Non-ceramic insulators, also called composite or polymer insulators, were utilized first in 1959 in North America [9]. Although the raw material cost of non-ceramic insulators is higher than that of ceramic materials [2], the non-ceramic insulators provide superior merits over the ceramic insulators including lightweight, smaller size, non-brittle, hydrophobic properties, lower surface area, and higher creepage distance. The lightweight and small size resulted in reduction in the installation and transportation costs, easier handling, breakage resistance, usage in narrow rights of way areas and visual aesthetics [1, 10, 2, 6]. The hydrophobic property, forming water beads on the surface, improved the performance under wet conditions. The longer creepage path with smaller surface area, that lead to higher surface resistance, enhanced the non-ceramic insulator performance under wet and contaminated situations [9]. It has been shown in both laboratory and field investigations that the performance of the non-ceramic insulators under wet and contaminated situations overcomes substantially the ceramic insulators [10]. Consequently, movement in the development of non-ceramic insulators were encouraged vastly by their excellent contamination performance [9].

At first, non-ceramic insulators were used as replacements for ceramic insulators in special situations including significant vandal incidents, limited right of way, and severe pollution conditions. Nonetheless, several issues were accompanied with their performance over the first two decades. For instance, they encountered several problems that affected the non-ceramic insulators performance like: tracking, chalking, erosion, and crazing of sheds, electrical breakdown and bonding failures along the rod-shed interface, separation of hardware leading to the fall of line, flashover, arcing, and water

penetration. Furthermore, corona could lead to sheds split [1, 9]. Hence, continuous research and efforts have led to improved non-ceramic insulators.

2.3.1 Main Components of Non-Ceramic Insulator

A non-ceramic insulator is mainly formed of a core, metal-end fitting, and weathersheds. Based on the design of the metal-end fitting and the core size, the two common types of the non-ceramic insulators are the suspension/dead-end type and the post type, as illustrated on Figure 2.3. The former is utilized where the core is subjected to tension forces by conductor weight. The latter, which is much larger in the core size, is used where the core is subjected to cantilever forces [1, 11].

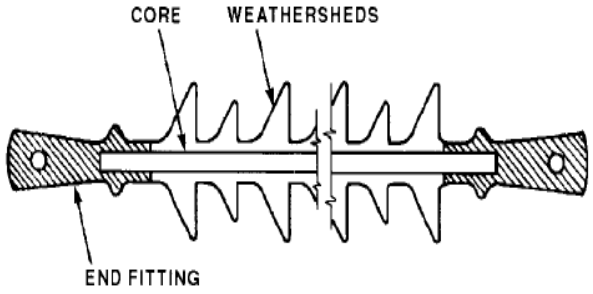

(a)

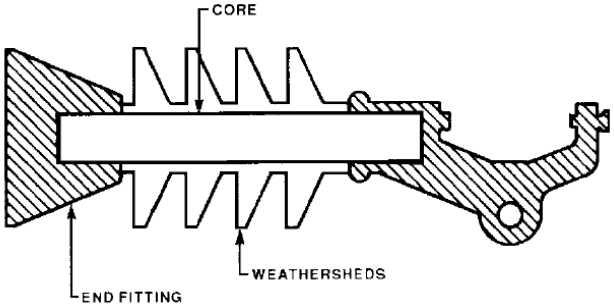

(b)

Figure 2.3. The non-ceramic insulators types; (a) suspension/dead-end and (b) post designs [11].

Insulator Core

The core provides two primary functions as it acts like an electrical insulator between the two end fittings and holds the mechanical load. For the aforementioned common types, the core contains axially aligned, glass fiber-reinforced resin such as epoxy or polyester [1].

End Fittings

The metal-end fitting is made of aluminum, forged steel, or malleable iron. It is provided as the attachment means of the insulator to the overhead line and to the support structure [10]. It is imperative to provide the core with proper end seals to prevent the fiberglass rod to come into contact with pollutants and moisture. Otherwise, brittle fracture of the core can occur resulting in insulator failure. Making end seals by molding the sleeved core onto the hardware is definitely the best type of seals due to the physical bond obtained by the molding [1,10].

Weathersheds Materials

Weathersheds (housing) surround the core to protect it from the combined effects of voltage and moisture and to provide electrical insulation between the end fittings [1,10]. In addition, the superior pollution performance is secured by the weathersheds providing the extra leakage path. The extra leakage distance can be acquired by adjusting the number and the diameter of the sheds [12].

Sheds are made from epoxy resins, including bisphenol-A epoxy and cycloaliphatic epoxies, polymer concretes, polyethylene, ethylene-propylene rubber, Teflon (PTFE), or silicone rubber. Each material provides specific properties [1, 10].

Earlier, General Electric Company developed the GEPOL insulator based on the bisphenol-A epoxy material which was applied in 1959. However, it failed due to erosion, tracking, and insufficient ultraviolet resistance of the bisphenol-A epoxy which was substituted by cycloaliphatic epoxies [10].

The cycloaliphatic epoxies with silica filler were provided to enhance the tracking resistance. However, their surfaces were deteriorated by UV radiation under outdoor conditions leading to chalking [10]. Currently, cycloaliphatic epoxies with various formulations are provided. Although they show successful long-term performance in normal conditions, their performance in polluted conditions is still unsatisfying [9].

The insulators constructed with Teflon housing material showed high erosion and tracking resistance under both wet and polluted environment. However, the bonding of the Teflon sheds to the core and to each other was insufficient which produced voids across the core that led to disastrous failures.

Therefore, the Teflon insulators designed for the transmission system were abandoned and replaced completely by silicone rubber (SiR) insulators [10].

The ethylene-propylene rubbers (EPRs) have been utilized widely as overhead insulators and classified into three types. They are ethylene-propylene monomer, ethylene-propylene diene monomer (EPDM), and a blend of ethylene-propylene and silicone (ESP). Initially, EPRs sustained tracking but did not possess enough resistance to UV radiation. Presently, EPRs with new formulations can resist both tracking and UV radiation. In clean locations, their performance for long-term are satisfactory. On the other hand, their long-term performance in polluted sites is still debatable [13].

2.4 Properties of Silicone Rubber Material

The silicone rubbers have been used successfully in overhead line applications and have showed excellent performance in different environmental conditions. Consequently, it is the most widespread polymeric material used in electrical power systems [1]. Silicone rubber insulators are approved as standard outdoor insulators for voltage rating up to ± 500 kV DC and 765 kV AC [13]. They are prepared from alternating siloxane linkage (Si-O) connected with methyl (CH_3) to construct polydimethylsiloxane (PDMS) [15], Figure 2.4.

The silicone rubber material is accompanied with merits and demerits. It exhibits proper resistance to corona, UV, weathering, ozone, majority of chemicals, and nearly all kinds of oils and waxes. Furthermore, the incentive for increasing of SiR in outdoor insulators applications is its unique ability to possess hydrophobicity. In addition, the silicone rubber insulation works safely when temperature is between -55^{o}C and 200^{o}C [13]. On the other hand, SiR is affected by intensified acids, aromatic solvents, intensive steam, and halogenated hydrocarbons [13]. In addition, the cost of silicone material is high resulting in impeding the replacement of ceramic suspension insulator strings [10].

The silicone rubber material is usually mixed with fillers like silica and aluminum trihydrate (ATH) to improve its physical properties [13]. For instance, silica can achieve desired mechanical properties of the material while ATH can inhibit flame and improve the resistance to tracking and erosion [10, 16]. When the temperature of the SiR surface filled with ATH exceeds 200 °C through surface arcing, water of hydration is released from ATH leading to the endothermic reaction which decreases the temperature of the surface and then assists in the extinction of the surface arcing [12].

The silicone rubbers used as HV insulation are classified into three types: high temperature vulcanized (HTV), room temperature vulcanized (RTV) and liquid silicone rubbers (LSR) [9]. The HTV silicone rubbers are vulcanized under high temperature. The vulcanization process of HTV rubber is by the action of heat and a peroxide (a vulcanizing agent) [13]. The RTV silicone rubber is converted from liquid into a solid rubber by curing. The RTV silicone rubber can be cured as either one-component system or two-component system. The former is vulcanized by diffusion of moisture from the air without other initiators. The latter is cured through other catalysts such as hydrosilylation [12, 17]. The third type of silicone rubber, LSR, is always cured by two-component system at high temperatures [12].

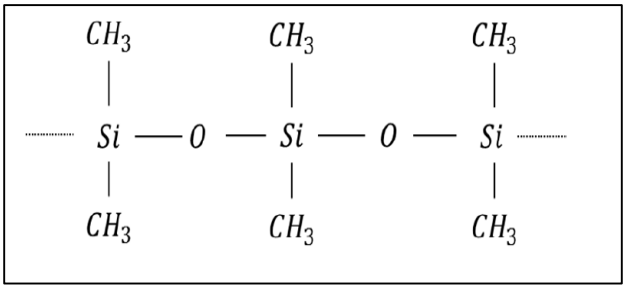

Figure 2.4. Molecular diagram of the PDMS [15].

Each type of silicone rubber material possesses certain advantages and disadvantages. Non-ceramic insulators based on RTV SiR were applied to transmission system in 1967. It was proven that they exhibited hydrophobicity, preventing leakage current, and performed well under contaminated conditions. However, erosion of the housing occurred leading to the exposure of the core. Thus, those insulators were replaced with HTV SiR insulators with ATH fillers to improve the resistance to the tracking and erosion [10]. Currently, the RTV SiR is used as coating on ceramic insulators to provide hydrophobicity and enhanced performance in polluted areas [13].

Beside the utilization of HTV SiRs as the material of the outdoor HV insulators, they are utilized on ceramic insulators as the extra extended sheds to reinforce their dielectric integrity and performance under pollution conditions [13]. Since the HTV SiR possess low fluidity and is solid prior to curing, long duration and a lot of pressure are required to achieve injection molding.

On the other hand, LSR SiRs, which have a smaller molecular weight and are liquid before curing, have a higher fluidity than the HTV SiRs resulting in simple injection molding process. This benefit

has spurred in the increase in research and utilization of LSRs for HV external insulation a short time ago [18], albeit they are still new [9].

2.4.1 Hydrophobicity of Silicone Rubber

Hydrophobicity of a non-ceramic insulator is one of the significant properties controlling the insulator surface conductance [13]. A hydrophobic surface causes water to be drops and obstructs the complete surface wetting. This can alleviate the leakage current, so the formation of the dry band can be prevented. Moreover, hydrophobic insulators have higher discharge inception voltages under wet and polluted conditions and higher flashover voltages compared with hydrophilic insulators [5, 13].

As a result, the hydrophobicity is a trait which makes SiR exhibits the prominent contamination performance [13]. It was shown in service that the performance of SiR in polluted locations overcomes EPDM [9, 19]. If the EPDM undergoes electrical discharges such as corona discharge, the EPDM surface can become permanently hydrophilic [20]. In contrast, if the SiR undergoes similar conditions and becomes hydrophilic, its hydrophobicity recovers when the stresses are sufficiently alleviated [21, 20].

The recovery of the hydrophobicity is primarily controlled by two factors. The first factor is reorientation of hydrophilic groups far from the affected surface. The second factor of the hydrophobicity recovery is the diffusion of the low molecular weight (LMW) polymer chains to the surface forming a thin layer of silicone fluid [13]. The LMW siloxanes are formed from the process of polymerization, processing aids which are silicone liquids, or from the exposure of PDMS to heat or electrical discharges [22]. The hydrophobicity loss and hydrophobicity recovery can be quantified to assess the severity of the aging process of SiR insulators.

2.5 Aging Processes in Silicone Rubber Insulators

During the operation of non-ceramic insulators, an imperative factor which must be regarded is the potential changes in electrical and mechanical properties through the aging phenomenon. The aging is defined as the attenuation of the performance with time due to encountered stresses [6]. Ultimately, the aging process may lead SiR insulator to complete failure [10]. That degradation of the SiR housing due to aging may cause exposure of the fiberglass rod to the environmental stresses, thereby the failure of the insulator [6].

The aging of SiR insulators relies on several factors. Some of these factors are related to weather, while others associated with system conditions including mechanical loads and electrical discharges. These factors can also have a combined effect, which can exacerbate the aging process [9, 6].

2.5.1 Environmental Factors

When the SiR surface suffers the long-term effects of climatic and operational stresses, reduction in its water repellency and several variations in both the surface morphology and chemical composition of the SiR are occurred. Generally, these variations exist at the top few monolayers [6]. The aging speed of SiR insulators can be significantly influenced as long as they undergo environmental stresses including relative humidity, pressure, temperature, ultraviolet radiation, and accumulation of pollutants and other chemicals [13]. These factors can lead to breakdown of macromolecules of polymers resulting in a reduction in molecular weight, from which the properties of polymer such as dielectric strength decreases [6].

Silicone rubber insulators perform well under polluted sites, especially where the pollutant is desert sand, road salt, or sea. The pollutant in these sites does not stick firmly to the surface of the SiR. Furthermore, the accumulation of the pollutant is minimized by periodic wind or regular rain cleaning. Therefore, regular insulator washing is typically not important. Nonetheless, the washing can be required to regain the insulation strength in some areas where wetting occurs for protracted periods [10].

2.5.1.1 Ultraviolet Radiation

When outdoor non-ceramic insulators, based on organic materials, exposed to UV rays, the organic materials suffer photo-oxidation and photolysis [7]. The high level of ultraviolet rays can produce changes in the material physical and chemical properties [4]. However, a silicone rubber polymer-based material is less susceptible to UV radiation. This can be attributed to the Si-O-Si bonds that are very stable to both UV and temperature [7]. Nevertheless, LMW components that comprise methyl groups (CH_3) are susceptive to absorb UV energy leading to the photoreactions which further cause aging.

It was proved experimentally that the SiR material is degraded by long-term exposure to UV radiation leading to physiochemical reactions which cause chemical and physical changes [4, 23, 24-26]. An example of the chemical changes is that UV radiation will break Si-C bonds and lead to substitution of carbon with oxygen. As a result, the carbon percentage will fade and the oxygen percentage will

increase which will cause the hydrophobicity loss [4, 27]. Khan demonstrated the dependence of O_2/C ratio on the intensity of UV-A radiations after an aging test [4]. Also, the rate of the hydrophobicity recovery would be reduced by the UV radiations, although the recovery pace is still faster in irradiated SiR than irradiated EPDM [18, 28, 29]. To illustrate the physical changes of the irradiated SiR, the UV rays can raise the surface roughness of SiR [18, 23, 26, 28] and pulverize the SiR [28]. In addition, small holes were observed on the surface of the irradiated SiR after performing UV aging test [18].

Terrab *et al.* indicated that the UV radiation has a crucial impact of SiR insulators in areas that suffer from high intensity of UV radiations such as the gulf region. Consequently, they recommended regular inspection to investigate the performance of non-ceramic insulators utilized in these areas [27]. However, a disputable point was made by Venkatesulu *et al.* who simulated the accelerated UV weathering conditions of SiR insulators and reported that the UV radiation had no significant influence on the SiR. They concluded that SiR possesses a great long-term resistance against UV rays [30].

2.5.1.2 Humidity

One of the environmental factors that is considered during the SiR design is humidity. For illustration, the surface conductivity of the SiR insulator would increase if it encounters mist or fog [7]. It was observed that the SiR cannot significantly prevent permeation of water vapor in humid conditions [61]. Therefore, moisture may diffuse into the bulk of SiR housing, and be in the shape of bound water and unbound water within the housing. The former is attached to the filler particles surfaces due to hydrogen bonding or the van der Waals force. The latter, on the other hand, occupies the pre-existing voids or the free volume in the SiR. The moisture within SiR causes growth in polarization charge, , the dielectric constant and reduction in AC breakdown field strength and the volume resistivity of SiR [59].

In the event that the quality of the sheath-core interface is insufficient, a water vapor from the humid environment may permeate into the glass fiber-reinforced resin core. The core tends to absorb water and undergoes degradation mechanisms including the following: hydrolysis, ion exchange, partial discharges, or the core corrosion [60-62]. Consequently, the absorbed water leads to variation in electrical and mechanical characteristics of the core resulting in a brittle fracture [60].

2.5.1.3 Temperature

The ambient temperature can be considered as one of the major aging factors of SiR especially under long-term dry conditions like arid environment [30]. It was observed experimentally that thermal aging of SiR under dry conditions resulted in surface oxidation, surface roughness [63] and decrease in ATH content [66]. Nonetheless, mechanical stress capacity of the SiR insulator increases by thermal aging under arid environmental conditions [63]. Also, since surface free energy reduces with growing temperature [64], increase in temperature leads to increase in the hydrophobicity recovery rate [65].

The SiR has flexible and strong linking between alternating Si and O atoms and organic groups exhibiting high oxidation resistance and superior resistance to thermal degradation and UV [7, 16]. Venkatesulu and Thomas conducted long-term accelerated weathering experiment on SiR insulators and concluded that SiR insulators under desert conditions are able to perform well over many years [30]. Khan investigated the performance of SiR insulators under simulated conditions of arid desert including temperature and different intensities of UV. In his work, the author observed noticeable surface roughness of SiR insulators. Moreover, prominent surface degradation was produced in the SiR insulators exposed to UV rays of 4 mW cm^{-2} that was the highest UV intensity used in the author's study [4].

Synergistic effects of environmental factors, including UV, temperature, and humidity, and the electric stress on SiR insulators have been analyzed by Verma *et al.* They found that those stresses produced the SiR insulator surface degradation and dry band discharges as well as growth of the measured leakage current. Furthermore, they assessed tensile strength of the aged SiR slabs, and they reported reduction in breakpoint extension of the aged samples implying brittleness created by UV [31].

2.5.2 Electrical Factors

Electrical factors, in the form of electrical discharges, are the aging factors associated with system conditions. The electrical discharges can be in the shape of dry band arcing or corona.

2.5.2.1 Dry Band Arcing

One of the major electrical sources of ageing is the dry band arcing originated from the flow of leakage current. The development of the leakage current over the surface is suppressed by the hydrophobicity of SiR surface preventing coalescence of water drops that forms a continuous path. Nevertheless, the leakage current develops when the surface is significantly wet, or a pollutant layer

accumulates during period of hydrophobicity loss [10]. The leakage current heats up the electrolytic layer on the surface. Since the current density as well as the power dissipation along the surface is not uniform, the heat dissipation evaporates water in the higher current density regions leading to the formation of the narrow dry bands. Hence, substantial variation in the voltage distribution along the insulator occur resulting in dry band arcing in the form of electrical discharges that bridge the dry bands [57]. Such discharges generate the localized hot spots which cause erosion of the silicone insulator housing [10, 11]. Hence, employing inorganic fillers including ATH and silica is needed to enhance the thermal conductivity of the SiR. Those fillers assist in removing heat from the localized hot spots to lower temperature of the hot spots, thereby inhibiting the erosion [58].

2.5.2.2 Corona Discharge

The other electrical source of ageing is corona discharge, a form of partial discharge in a gas such as the air around an electrode when the electrical stress exceeds the dielectric strength of the gas. Design of equipment which prevents corona permanently at nominal voltage is usually uneconomical, especially in high voltage systems. Such corona activity causes several demerits including audible noise, radio interference, and power losses [13]. Also, corona can adversely affect non-ceramic insulators such as SiR insulators.

2.6 Effects of Corona Discharges on Silicone Rubber Insulators

Silicone rubber insulators exposed to corona encounter concurrently a mixture of energetic particles and radiation, including ions, electrons, ozone, high temperature, and UV [5,32]. Under the corona exposure, various chemical reactions occur including the following: (a) growth in the oxygen content by generation of hydroxyl and silanol groups [33], (b) oxidative crosslinking [34], and (c) degradation of the silicone rubber network structure that leads to diffusion of low molecular weight siloxanes [35]. Such reactions cause variations in mechanical and electrical properties of the SiR surface along with exposure of fillers [5]. The chemical reactions accompanied with corona exposure on the SiR surface are summarized below [32]:

(i) Corona establishes scissions of chain segments (Si-O-Si, Si-CH_3, and C-H groups) leading to form free radicals (Figure 2.5).

(ii) Active oxygen atoms and ozone are produced (Figure 2.6).

(iii) Due to the active oxygen and hydrogen atoms and free radicals, silanol groups (Si-OH) containing hydrophilic hydroxyl bonds are formed, as illustrated in Figure 2.7.

(iv) Condensation and dehydration reactions of the silanol groups occur, as shown in Figure 2.8.

(v) The chemical bonds between Si and O are created by the active oxygen, as depicted in Figure 2.9.

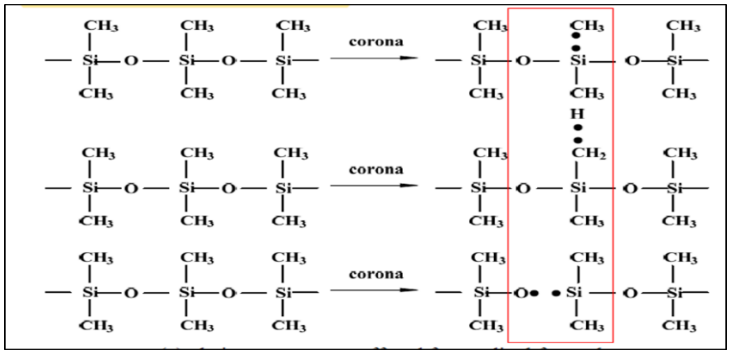

Figure 2.5. Formation of scissions of chain segments and free radicals by corona [32].

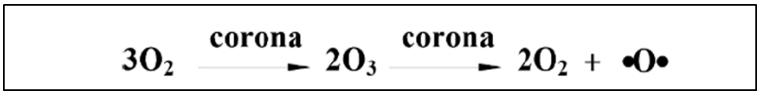

Figure 2.6. Generation of ozone and active oxygen atoms during corona exposure [32].

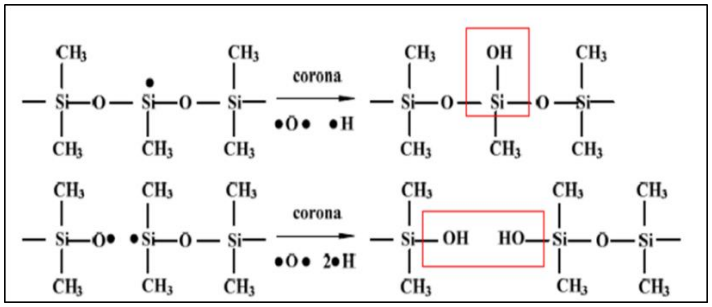

Figure 2.7. Si-OH groups created under corona discharges [32].

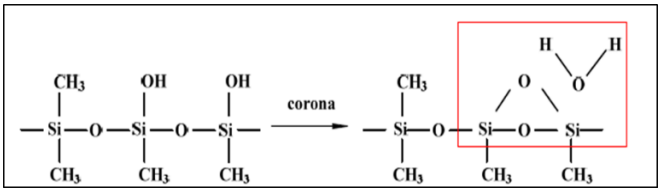

Figure 2.8. Dehydration and condensation reactions under corona discharges [32].

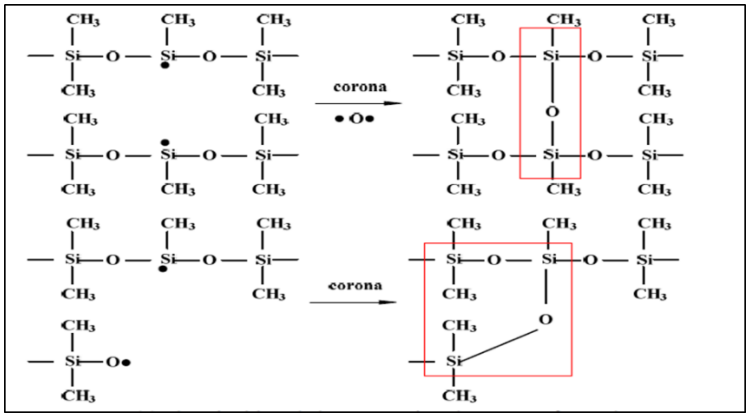

Figure 2.9. Chemical bonds between Si and O established by corona discharges [32].

After the SiR is exposed to corona, silica-like surface, which is hydrophilic, appears. In addition, water molecules are absorbed by the hydroxyl (silanol) groups. Then, hydrogen bonds form between the absorbed water and the hydroxyl groups, as represented in Figure 2.10. The silica-like layer, silanol, and chemically absorbed water that appear on the SiR surface during corona discharges are considered as hydrophilic factors. Such factors lead to the hydrophobicity loss of silicone rubber insulation [32]. Those repercussions of corona discharges have attracted attention of researchers.

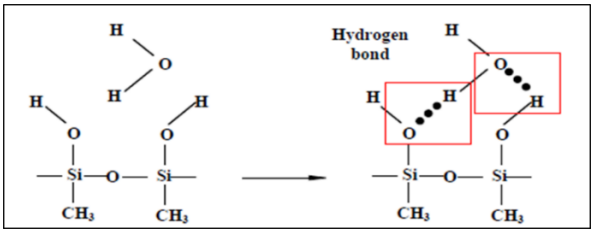

Figure 2.10. Chemical absorption of water [32].

2.6.1 Field investigations

In the field, corona discharges are initiated by either degraded or improperly designed corona rings or water droplets on the insulator surface. The former stems from the sharp points and affects only the insulator parts that are close to the electrodes. Nonetheless, it is avoidable by appropriate design of corona rings. The latter originates because of differences in permittivities between the water drop, SiR, and air, that results in enhancement of the electric field at the triple point. These regions behave as discrete and distributed sources of corona that promotes ageing at different parts of the insulator [36]. Examples of SiR surface damage due to corona is depicted in Figure 2.11. The eroded housing can lead

to the exposure of the fiberglass rod to moisture. The exposed core could deteriorate by brittle fracture, erosion, or tracking, resulting in complete insulator failure.

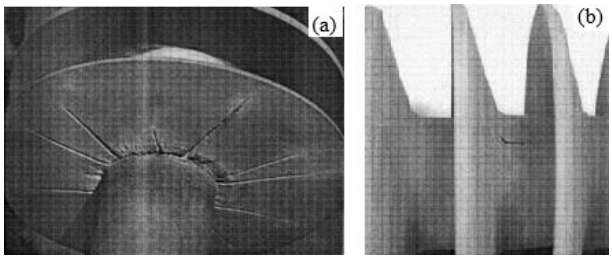

Figure 2.11. Corona cutting of the weathersheds of two different 230 kV non-ceramic insulators without corona rings in two various degradation phases: (a) the advanced phase; (b) the early phase [38].

Some investigations were performed to analyze the behavior of SiR insulators under corona discharges in the field. Philips *et al.* analyzed the influence of water droplets corona on a 400 kV SiR insulator removed from service. They found that the magnitudes of electric field on the sheaths of the investigated insulator surpassed the water drop corona threshold. Furthermore, whitening of the surface was noticed. Moreover, permanent hydrophobicity loss near the high electric field regions was observed [39]. Reynders *et al.* stated that the major ageing factors of SiR surfaces in service are due to corona and local arcing [40].

Umedaet *et al.* investigated a SiR insulator without corona ring that aged in the field, and they observed severe rubber aging on the line side as presented in Figure 2.12 [44]. On the other hand, there was no noticeable deterioration at the ground side of the insulator. Also, SiR insulators equipped with corona rings utilized in the field were not aged severely. It was shown through FTIR analysis that the aged insulator contained nitric acid. Based on those observations, they deemed that corona discharges under polluted and humid conditions generated the nitric acid. According to Kumosa *et al.*, the formation of nitric acid originated by activities of water droplets corona as well as partial discharges at the rod to housing interfaces in the presence of moisture is the most potential source of brittle fracture failure [41-43].

Figure 2.12. Deterioration on the aged silicone rubber insulator [44].

2.6.2 Laboratory analyses

Since the random distribution of the water droplet corona as well as uncontrollable intensity of the corona discharges noticed in the field investigations, different artificial tests producing controlled corona discharges from diverse setups have been provided [45]. Among such methods, the one depicted in IEC 60343 standard can be employed to investigate the corona resistance [46]. The method is based on a cylinder-plate electrode configuration that forms discharges on a surface of a material sample until a breakdown occurs and the time until a breakdown is recorded. The drawback of such procedure is that the created discharges are a blend of capacitive coupled gliding discharges and corona [45].

Another configuration of the corona test, known as a needle-plane setup, is used in many experimental studies to investigate the effects of corona discharges on a SiR material [37, 47, 48]. The results of these studies showed that the corona discharges can cause physical and chemical changes to the SiR surface. Perceivable cracks on the surface of SiR were detected by means of scanning electron microscopy (SEM) images [37, 47, 48]. Through Fourier transform infra-red (FTIR) spectroscopy, the broadening of Si-O-Si peak was indicated, characterizing oxidative crosslinking of SiR material by corona discharges [47]. Moreover, the FTIR analysis demonstrated that the intensity peak of Si-CH_3 receded, while the peak in the OH region broadened. These observations indicated formation of the hydrophilic groups (OH). Thus, the corona discharges could transform the hydrophobic surface of SiR into hydrophilic surface, albeit impermanent [37, 47, 48]. It was shown by thermogravimetric differential thermal analysis (TG-DTA) that corona can generate dehydration phenomenon in SiR materials [37]. Bao *et al.* performed X-ray photoelectron spectroscopy (XPS) analysis on SiR specimen exposed to corona [32]. The results of these scans revealed that the exposure of corona discharges could lead to surface oxidation, creation of silica-like layer, attenuation of the hydrophobic Si-CH_3 groups on

the surface, appearance of some C-O and C=O bonds, the production of Si-OH groups, and formation of chemically absorbed water molecules [32]. However, the ratio of Si-CH_3 rises steadily after the corona cessation resulting in hydrophobicity recovery. Such recovery arises from the diffusion of the LMW silicone fluid [48].

It was shown experimentally by Ma *et al.* that corona discharges are able to generate ozone from the SiR surface [36]. They also evaluated electrical and mechanical properties of SiR specimens by surface and volume resistivities, dielectric response (DR), tensile strength, and elongation at break. They found that the surface resistivity was highly sensitive to the corona treatment. Nevertheless, the volume resistivity as well as DR showed an insignificant vulnerability to the corona exposure. Based on the mechanical assessment, the SiR specimens affected by the corona discharges exhibited small reduction in the tensile strength and the elongation at break. This observation was elucidated that the corona discharges can deteriorate a surface of SiR insulation, whilst the volume matrix of the silicone rubber remains uninfluenced.

The impingement of corona discharges on SiR insulators depends on the applied voltage type, i.e., AC corona or DC corona. The influence of the AC corona, compared to the DC corona, on SiR material is higher [32, 36, 49-52]. Moreno and Gorur compared the impacts of AC and DC corona discharges on polymeric housing materials as surface charge, and they recorded considerable lower magnitudes of surface charge after the AC corona treatment, compared with the DC corona treatment [53]. According to Ma *et al.*, the intensity of DC corona discharges is affected by the electrostatic charging of the polymeric surfaces which results in attenuation of electric field distribution across the discharge regions. Hence, they found that its discharge intensity was less than that of AC corona. Such differences in the corona discharge intensities generated significant changes in ozone production which was higher when SiR material was exposed to the AC corona. In addition, the AC corona treatments had higher impingement on surface resistivity of the silicone rubber material than the DC corona treatments. Based on the XPS and FTIR analyses, it was shown that there was a lesser tendency for the surface oxidation for the DC corona treated samples as compared to the AC corona treated samples [36].

The corona discharge under AC voltage was compared with the DC corona on the same test conditions employed in [32, 49]. Based on the investigation performed by Bao *et al.*, the AC corona reached the whole surface of SiR samples, whereas the DC corona appeared along applied electrode. As a result, the power released from the former was greater than that from the latter. Furthermore, the

DC corona treatment generated less chemically absorbed water on the SiR housing surface than the AC corona treatment. Moreover, the impingement of the AC corona on the SiR material was much worse than that of the DC corona in connection with the hydrophobicity loss [32]. According to Reddy and Prasad, no noticeable cracks appeared on the DC corona treated SiR specimens presented on the SEM illustrations, unlike the AC corona treated SiR specimens [49]. Those investigations that showed more severe effect due to the AC corona, in comparison to the DC corona, motivated the selection of the AC corona to be investigated in this research.

The corona discharges can combine with another stress to produce synergistic effects on silicone rubber insulators leading to acceleration of the insulator degradation. To illustrate, the properties of the SiR materials exposed to corona discharges under humid conditions were investigated and compared with the SiR materials exposed to corona discharges under normal condition in [49, 52]. Compared with the normal condition, a higher hydroxylation of SiR samples was created by corona discharges under the high humidity condition as shown by FTIR analysis. Moreover, formation of nitric acid on surface of the treated specimens under the humid state was detected by FTIR spectrum and gaseous byproduct measurement through gas analyzer [49 ,52]. The corona impacts on SiR samples were compared in terms of the different conditions through SEM analysis by Reddy and Prasad [49]. It was stated that minor cracks were connected to the main crack on the surface under the normal condition, whereas cracks under the high humidity condition were scattered throughout the surface of the specimens, especially the treated region. The authors hinted that corona discharges under the high humidity condition have stronger effects on the surface than that under the normal condition based on the SEM analysis [49]. Interestingly, illustrations of the SEM analysis depicted that the corona under the normal condition originated more severe cracks as compared to the high humidity condition, although the paper did not discuss this observation.

Combined influence of corona discharges with humidity and mechanical stress were studied by Moreno and Gorur [54]. They found that the intensity of degradation of the SiR housing material increased with the level of humidity and presence of mechanical stress. Micrographs of the samples were captured periodically during the test. Cracks on the surface of SiR samples were observed under all situations. The application of the mechanical stress raised depth of the cracks. Compared with the low humidity, the rate of the crack formation generally was slightly higher under high humidity. Furthermore, surface whitening was noticed on SiR material treated under the high humidity.

A function of acid fog as the contributing factor to the degradation of SiR materials exposed to the corona discharges was analyzed in [51, 52]. It was shown that the acid fog was more severe acceleration factor than that of the normal fog. The reason of this result was that the acid fog contains dissolved pollutants which increases the conducting medium for the corona discharges [51]. Based on FTIR analysis, formation of nitric acid on the surface of the SiR material exposed to the corona was more prominent under the acidic fog condition as compared to the normal fog. It was proven through EDX analysis that the oxidation and hydroxylation on the surface were more noticeable for the acid fog treatment, compared with the normal fog [51, 52]. Since the acid fog provided the highest corona intensity among the normal fog and normal air conditions, it was found that the hydrophobicity loss was worst under the acid fog. On the other hand, the rate of the hydrophobicity recovery was highest for the acid fog treatment. The authors interpreted that larger cracks, which weaken the resistance path, might result in higher diffusion rate of LMW components from the material bulk to the surface [51].

Du *et al.* investigated impingements of corona discharges on the surface of SiR insulation at various ambient pressures. They showed that variation in the ambient pressures induced diverse intensities of corona discharge, as well as different hydrophobicity losses, based on Paschen's law. As the air pressure was raised, the corona voltage decreased initially and then increased, i.e., the corona discharges intensity was raised at first and then dropped [55].

The behavior of corona discharges bombarding SiR under varied wind conditions was studied in [56]. It was proven that the corona discharges were intensified by the vertical wind and inhibited by the parallel wind which could take the ions away from the SiR surface. These phenomena could be strengthened by increase in the wind speed. For illustration, it was observed that the number of current pulses, cumulate charge, and time-averaged current under the vertical wind condition increased as the speed of the wind increased. In contrast, they decreased under the parallel wind condition with the growth of the wind speed. It was found that the vertical wind strengthened the hydrophobicity loss and accelerated the hydrophobicity recovery. On the contrary, the parallel wind weakened the hydrophobicity loss and inhibited the hydrophobicity recovery because the LMW polymer chains can be taken away by the parallel wind.

2.7 Summary of Literature Review

The aforementioned literature can be summarized as below:

- When the SiR surface suffers the long-term effects of climatic stresses such as UV, humidity, or temperature, several variations in both the surface morphology and chemical composition of the SiR are occurred.
- Corona discharges result in variations in chemical, physical, and electrical properties of the SiR surface.
- AC corona produces higher influences on SiR material in comparison to DC corona on the same test conditions.
- The corona discharges can merge with another stress including humidity, mechanical stress, acid fog, pressure based on Paschen's law, or vertical wind to produce synergistic effects on SiR insulators leading to acceleration of the insulator degradation.

To the best of our knowledge, synergistic effects of corona discharges and UV radiation on SiR insulators have not been investigated yet. Since the UV radiation can penetrate deleteriously the SiR surface, it was postulated in this study that such radiation can intensify the corona impact on the surface of the SiR insulation. Consequently, the following chapters are dedicated to explore deeper into that postulated issue.

Chapter 3
Materials and Methods

It is the keystone of this work to investigate the impacts of corona discharges on silicone rubber insulators under various environmental conditions including high humidity and UV rays. To execute this investigation, the methodology of the corona aging test is proposed in this study. This chapter is dedicated to provide the descriptions of the experimental configuration, the procedure to perform the test, and the techniques for analyzing the SiR specimens.

3.1 Corona Aging Test

3.1.1 General Assumption

The methodology in this work for testing the performance of the SiR material subjected to corona discharges under severe environmental conditions assumes that the examination should be executed in a chamber to simulate the environmental conditions. Further details of the experiment are elucidated below.

3.1.2 Experimental Setup

The schematic diagram of the test arrangement to investigate the corona impacts is depicted in Figure 3.1. The main elements of the test setup comprise of an isolation transformer, a variac, a step-up high voltage test transformer (120 V/ 16 kV,10 kVA), a HV probe with a ratio of 1000:1, two high frequency current transformer (HFCT) with 200 Hz - 500 MHz and 9.5 kHz – 1.5 GHz, and a digital oscilloscope with the bandwidth of 200 MHz with a sampling rate of 2.5 GS/s. The stainless steel chamber with a volume of 1 m^3 is employed to simulate the severe conditions, and it includes a corona electrode configuration, SiR samples provided by Poly-Nova Technologies, a humidity generator, a humidity sensor, and UVA lamps. The high voltage supply is connected to the chamber via the high voltage bushing. The environmental conditions are monitored through a computer equipped with a LabVIEW program and data acquisition system (NI USB-6001) that has 13 digital inputs/outputs, 8 analog inputs with 14-Bit and 20 kS/s, and 2 analog outputs with 5 kS/s/ch.

• Corona electrode

The corona electrode configuration was designed as shown in Figure 3.2. The configuration involves 6 pairs of HV stainless steel needle electrodes and grounded plane electrodes, on which the SiR samples

($5 \times 5 \times 1$ mm^3) are placed. The tip radius of each needle is around 0.02 cm [54]. The gap distance between the surface of the treated sample and the tip of needle is kept at 6 mm.

• Humidity generator

The humid condition inside the test chamber is simulated by humidity generation. An ultrasonic humidifier was utilized with capacity of 1/3 L/h. The humidity level is measured using a humidity sensor (HTM2500LF) with 0 – 100 %RH measuring range and accuracy of ±3%RH. Deionized water is used for the humidity generation to avoid the effect of mineral ions of water which can lead to arc discharges along the treated sample.

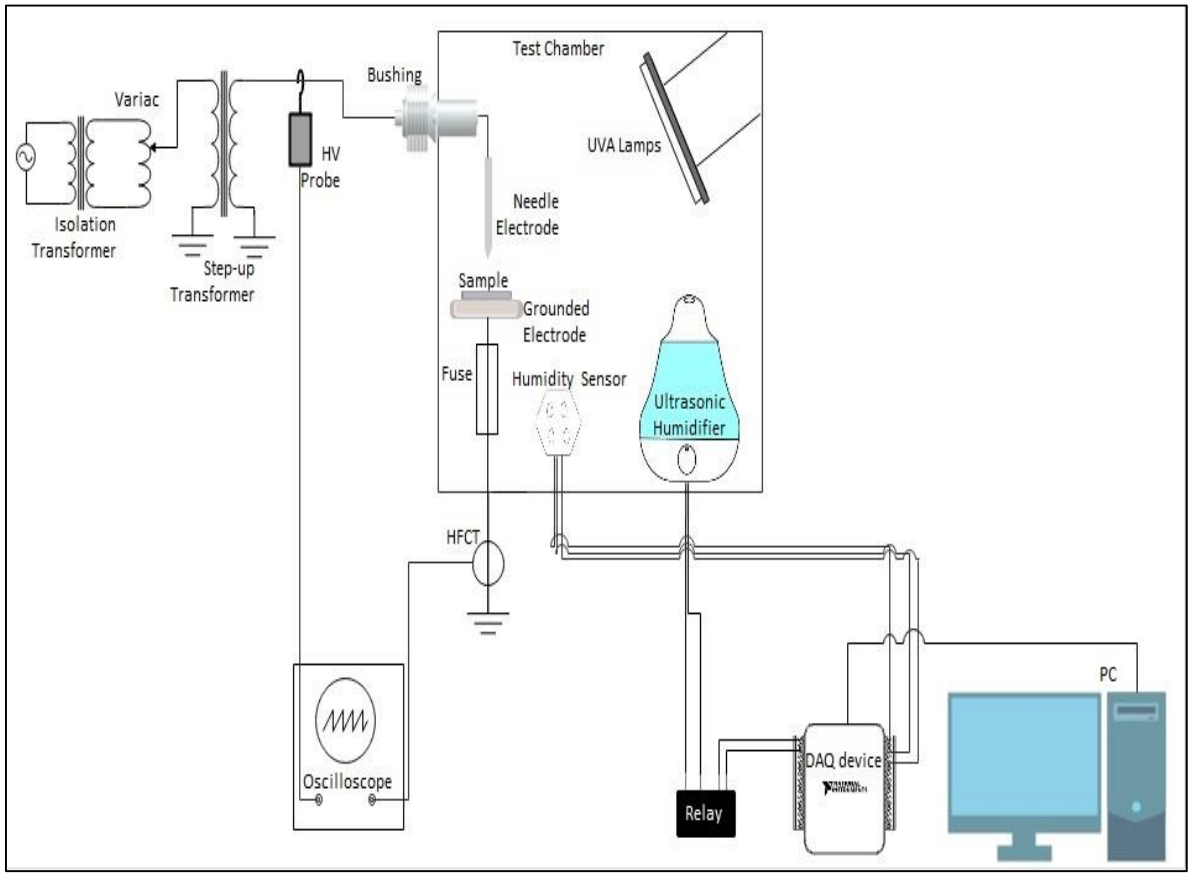

Figure 3.1. A schematic diagram of the test setup used in corona treatment under different environmental conditions.

Figure 3.2. The structure of six pairs of electrodes used in generating corona discharges.

• UVA lamps

The UV radiation inside the chamber should mimic the portion of the solar spectrum that leads to aging of the non-ceramic insulators. For this reason, the proper selection of UV lamp among available UV lamps on the market is significant in order to simulate the particular wavelength region of sunlight. Compared with different UV lamps, UVA lamps usually offer superior correlation with realistic outdoor weathering although they usually lead to slower degradation because they do not produce any UV output under the solar cutoff wavelength of 295 nm [68]. For this study, UVA-340 lamps were selected since they offer the greatest available simulation of sunlight within the critical short wavelength region (295 nm ~365 nm) as represented in Figure 3.3.

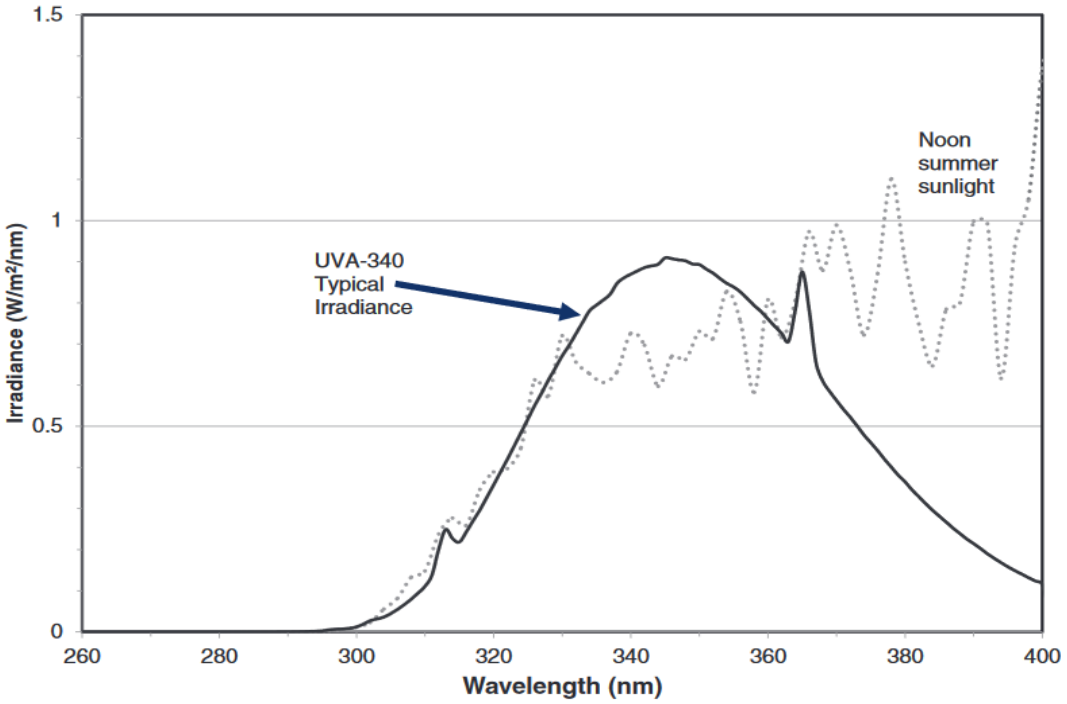

Figure 3.3. Comparison of sunlight and UVA radiation spectrums [68].

UVA-340 lamps with a length of 1.2 m were utilized to simulate UVA radiation impacting on the surface of SiR. The number of lamps and the spacing between them and the SiR samples were designed to ensure that the SiR samples under test would be stressed with an UV radiation of 1 mW/cm^2 which is the same light intensity recommended in the IEC 61109 [24, 69]. The intensity of UV radiation was measured using UVA/B Meter (UV513AB) with spectrum range from 280 to 400 nm and with illumination range from 1 to 9999 µW/ cm^2.

3.1.3 Experimental Procedure

For comparing the effects of various weather conditions in terms of accelerating the effect of 24-h AC corona on SiR, a 10 kV AC voltage was applied. The test procedure discussed in this section is proposed to assess the resistance of commercial SiR samples to the corona treatment under acute environmental conditions. The corona treatment was performed with and without UV radiation. Each of these cases was performed under three humidity conditions, i.e. high humidity (80 to 90%), medium humidity (55 to 65 %) and low humidity (<40 %). Thereby, six diverse environmental conditions were simulated in the test.

Twenty-one samples of silicone rubber were necessary to fulfill the entire test program. Three SiR samples were utilized for each weather condition. Each sample was cleaned by isopropanol alcohol prior to the experiment, and then dried for 1 hour at least at room temperature. Those specimens were characterized physically and chemically after 24 hours of the corona exposure. The above-mentioned procedure is achieved in cyclic mode for a duration of 24 hours. Each cycle proceeds for 1 hour. During one cycle, voltage is on during the whole experiment while humidifier is on for 30 minutes and off for 30 minutes. For low humidity condition, the humidifier is off during the entire experiment. During UV case, UVA lamps are on during the entire test.

3.2 Study Approach

3.2.1 Corona Current Measurement

Leakage current induced by the corona discharges at each environmental condition was captured by means of the high frequency current transformer placed around the grounding wire. The voltage across the electrode gap was measured with the high-voltage probe connected at the high-voltage side of the test transformer. The waveforms for those measurements were traced by an oscilloscope to indicate the existence of the corona discharges. The frequency band of corona discharges within air ranges usually between 0.150 to 5 MHz [36]. Therefore, the bandwidth of the employed oscilloscope was set at 200 MHz. The measurements were performed while placing a SiR sample on the grounded plane electrode. As illustrated in Figure 3.4, corona discharge current was captured during the experiment indicating the existence of corona discharges.

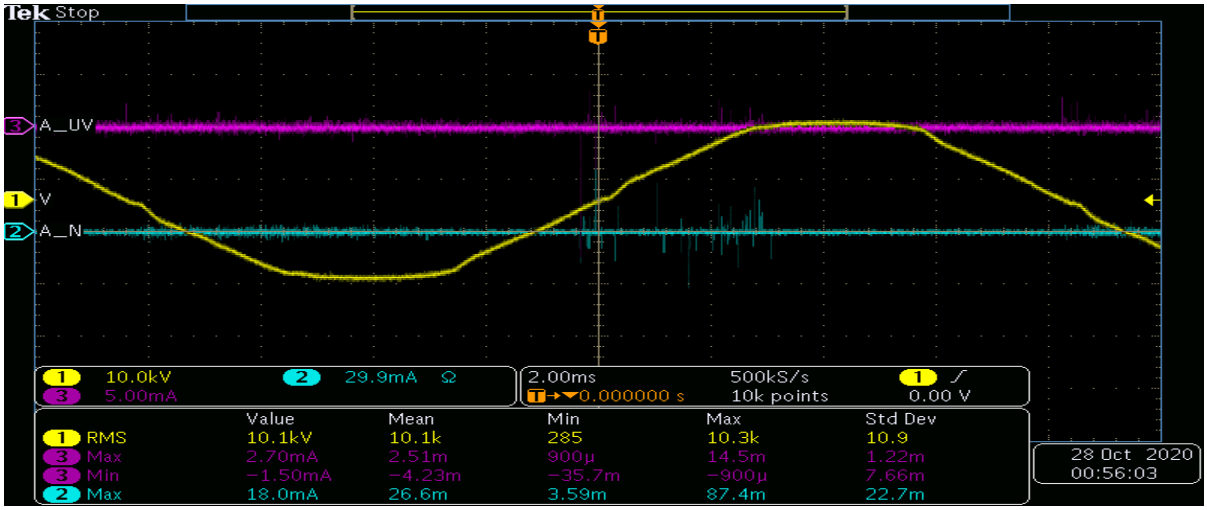

Figure 3.4. Corona discharge current under medium humidity

3.2.2 Hydrophobicity Loss and Recovery Measurements

As the aging process begins with the loss of hydrophobicity, it is important to evaluate the hydrophobicity of SiR. There are several methods to assess quantitatively the hydrophobicity loss and recovery such as static contact angle, dynamic contact angle, water soaking, sliding angle, and the Swedish transmission research institute scale [70]. The most widespread among them is measurement of the static contact angle which is at the interface between the material surface and a liquid drop that comes in contact with the material surface. The contact angle relates to the surface tension of the liquid and the surface energy of the solid via the following Young–Dupré equation [12]:

$$\gamma_{GS} = \gamma_{SL} + \gamma_{LG}.cos\theta \qquad (3.1)$$

where γ_{GS}, γ_{SL}, and γ_{LG} are the interfacial tensions between gas and solid, solid and liquid, and liquid and gas respectively, and θ is the static contact angle (identified in Figure 3.5).

Hydrophilic materials possess high surface energy and are readily wettable allowing water to touch a significant surface area and then make contact angle beneath 90°. In contrast, hydrophobic materials have low surface energy and inhibit water flow on their surfaces and thus make the contact angle exceed 90° [7]. The behavior of water drops on different types of SiR surfaces is illustrated in Figure 3.5.

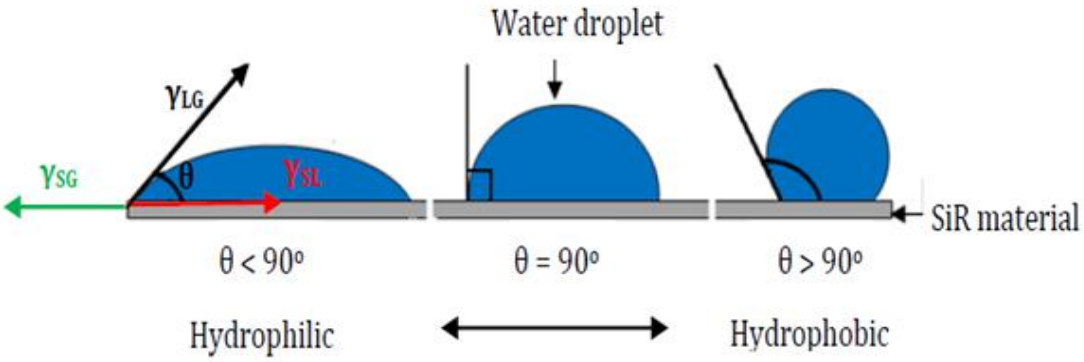

Figure 3.5. Water droplets on SiR samples with different degrees of hydrophobicity [7].

In order to evaluate the surface hydrophobicity by the contact angle method, a single droplet of 20 µl of distilled water was placed using a micropipette vertically on each SiR specimens' surface that was below the tip of needle during the corona treatment. Immediately after the droplet was deposited, a picture of the droplet was taken and transferred to a computer. Eventually, the static contact angle was

obtained from the picture using "ImageJ" software based on low-bond axisymmetric drop shape analysis approach [71]. The contact angle measurements were taken immediately after the corona treatment and during the recovery for 100 hours to evaluate the hydrophobicity loss and recovery respectively.

As represented in Figure 3.6, the contact angle analysis via software "ImageJ" generally assumes that the droplet is part of a sphere. In reality, the shape of the droplet is close to the sphere shape because of gravitational effect and molecular dispersion. Nonetheless, the effect of gravity can be ignored when the droplet size is small. The contact angle (θ) presented in Figure 3.6 is obtained as [29]:

$$\theta = 90^{\circ} - \tan^{-1}\left(\frac{r-b}{\sqrt{2rb-b^2}}\right) \qquad (3.2)$$

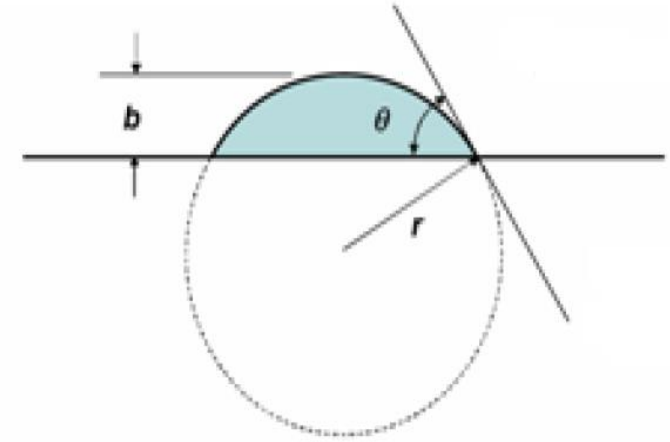

Figure 3.6. Theoretical model of a contact angle representation [29].

3.2.3 Scanning Electron Microscopy (SEM) with Energy Dispersive X-Ray Analysis (EDX)

SEM is a technique to acquire data for the surface topography to detect the morphological variations in the tested surfaces. To form SEM images, a specimen is scanned by a beam of high-energy electrons in a raster scanning pattern. The electrons in the beam interact with atoms of the specimen in order to produce signals that include information of the specimen in regard to the surface topography and composition. The SEM analysis was achieved using FEI Quanta Feg 250 ESEM system equipped with EDX detector to specify the elemental composition of the specimens.

In this work, the variation in surface topography of the SiR specimens exposed to the corona discharges was assessed through SEM analysis.

3.3 Summary

This chapter has described the materials and methods utilized for the current study. Particulars for the experimental configuration and the procedure to perform the corona test have been provided. Other components of this chapter described in detail comprise the techniques for evaluating the consequent changes in properties of the SiR specimens.

Chapter 4
Results and Discussion

Based on the experimental setups, methodology, and study approaches clarified in Chapter 3, the performance of the silicone rubber (SiR) materials was evaluated with regard to their resistance to corona discharges under acute environmental conditions. The experimental findings procured by contact angle measurements, SEM, and EDX analysis are reported and discussed in this chapter. The outcomes of the diverse climatic conditions are compared to identify the impact of both UV and/or humidity along with corona discharges on the physical and chemical properties of SiR materials.

4.1 Hydrophobicity Loss

The contact angle was measured before starting of the aging test and immediately after the test. It has been found that all SiR specimens lost their hydrophobicity after corona discharges exposure under all environmental conditions. Table 4.1 depicts the measured contact angles for the initial (untreated) and immediately after the aging experiment for all cases. It can be noticed that the impact of UV radiation with no other stresses on the samples in terms of hydrophobicity loss was minimum as the contact angle only dropped on average less than 3°. On the other hand, samples exposed to UV along with corona discharges suffered from an average reduction of contact angle value of 12.0°, 5.3° and 9.4° when tested with corona and without UV at high, medium and low humidity respectively. Hence, the synergistic effect of UV radiation and corona discharges is evident in the hydrophobicity loss.

Moreover, samples exposed to higher humidity when tested with both corona discharges and UV suffered from more reduction in the contact angle. On the other hand, samples tested only with corona discharges without UV exposure did not show consistent trend when exposed to different levels of humidity. The inconsistency of the variation may be attributed to the short corona test duration. It is also worth mentioning that the higher the humidity, the higher the contact angle measurement variation.

Table 4.1: Measured contact angles of SiR samples for the initial and immediately after the corona test.

Contact angle / Condition	Average value (°)
Untreated	99±1
Only UV	96.33±5.51
Low humidity without UV	34±4.36
Low humidity with UV	24.67±4.93
Medium humidity without UV	23.67±5.67
Medium humidity with UV	18.33±6.81
High humidity without UV	28.67±10.97
High humidity with UV	16.67±8.33

4.2 Hydrophobicity Recovery

To quantify the hydrophobicity recovery, the contact angle was measured over 100 hours following the corona tests, and the results are depicted in Figures 4.1 and 4.2. It is apparent that the static contact angles did not return to the initial value for all cases. When comparing samples treated at the same humidity conditions, it is evident that the samples' recovery rate is similar regardless if the samples were treated with or without UV as evident in Figure 4.1. On the hand, and as depicted in Figure 4.2, the higher the humidity, the faster the recovery rate was for samples treated at the same corona discharges and UV conditions. The time for the contact angel to reach 90° for all tested cases is depicted in Table 4.2. It is evident from Table 4.2 that while the contact angle for samples tested with high humidity took only 15 hours to reach 90°, it took more than 100 hours for samples tested under low humidity to reach to the same angle.

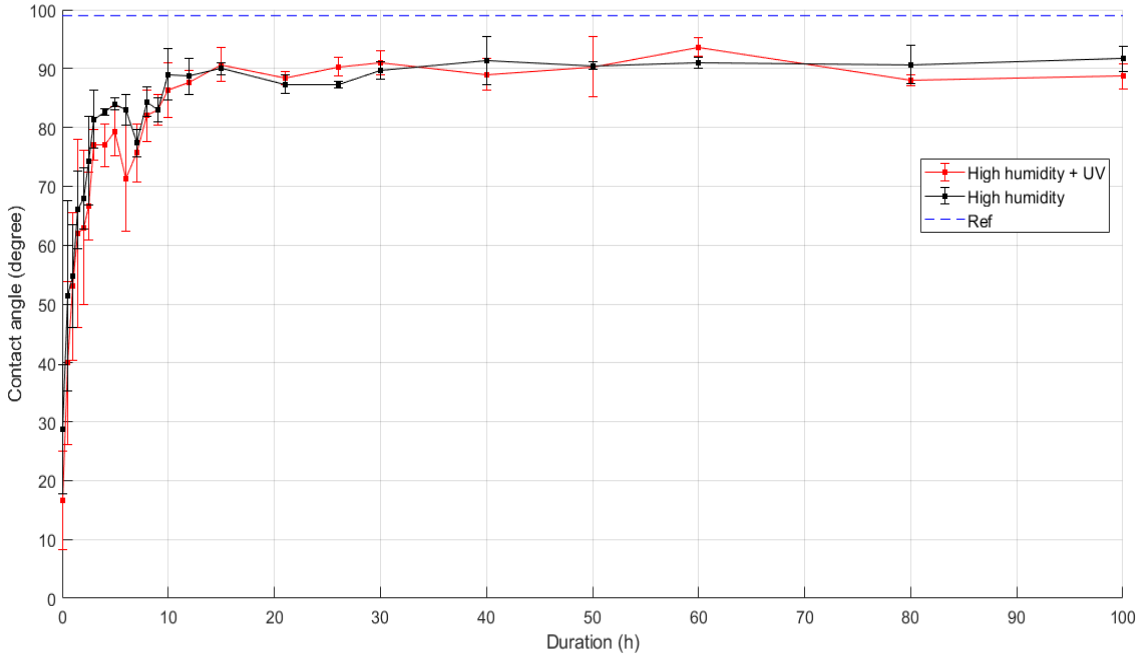
Contact angle (degree)
Duration (h)
High humidity + UV
High humidity
Ref

(a)

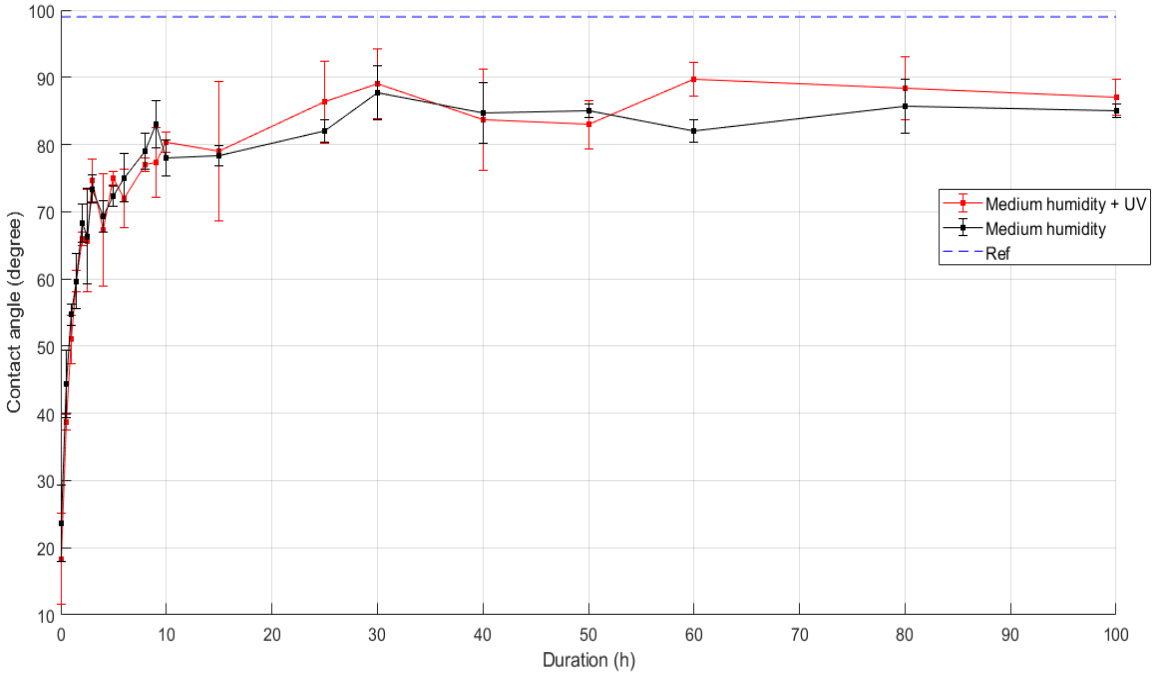
Contact angle (degree)
Duration (h)
Medium humidity + UV
Medium humidity
Ref

(b)

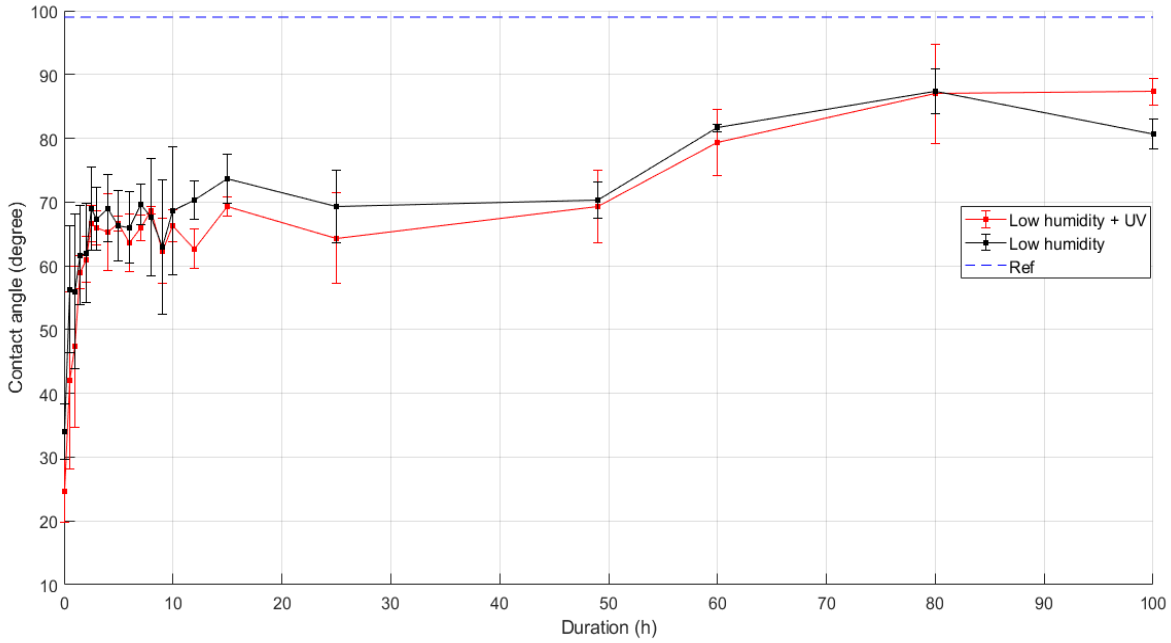

(c)

Figure 4.1. Hydrophobicity behaviour for SiR after the corona treatment with and without UV radiation under (a) high humidity, (b) medium humidity, and (c) low humidity.

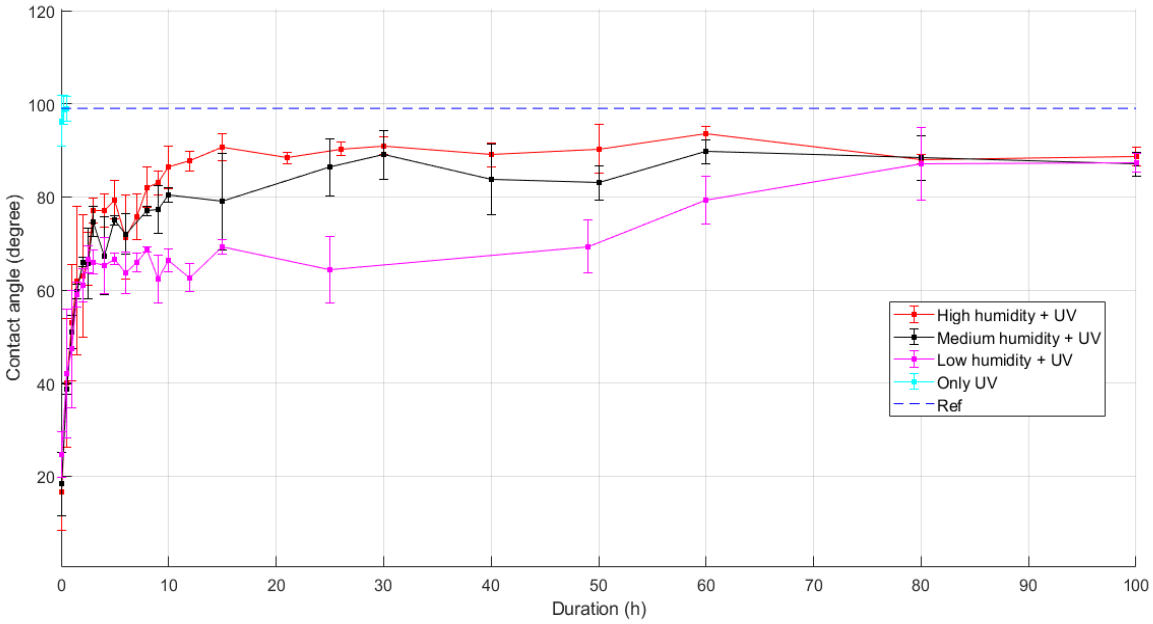

(a)

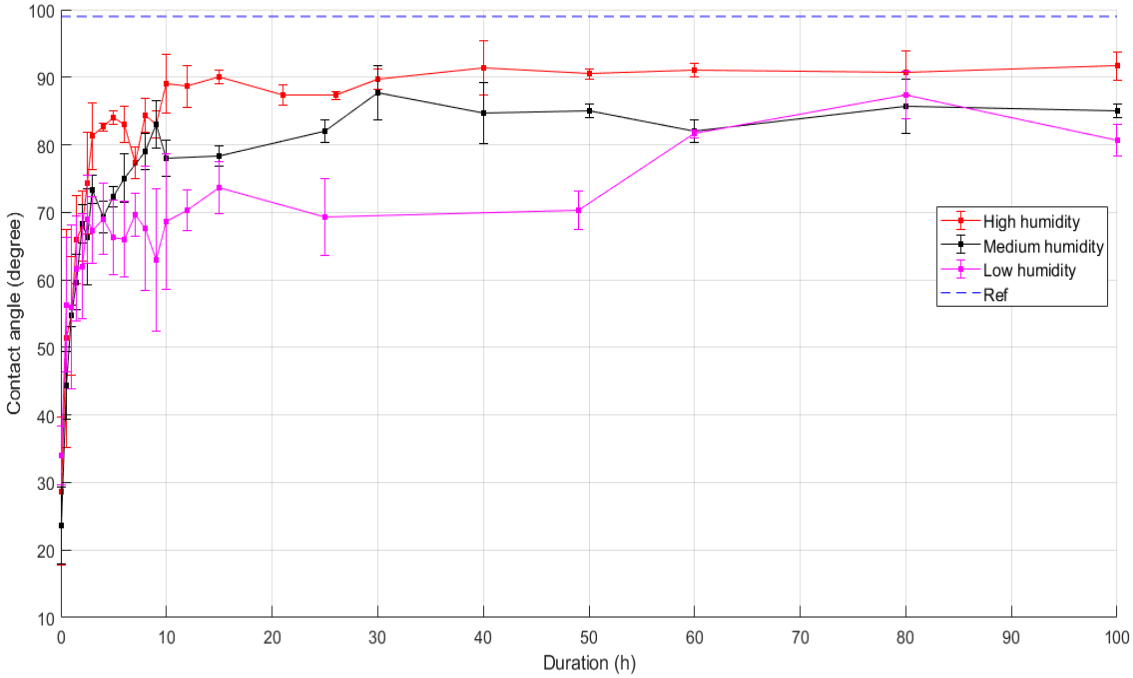

(b)

Figure 4.2. Hydrophobicity behaviour for SiR after the corona treatment under different humidity levels with (a) UV radiation and (b) without UV radiation.

Table 4.2: Recovery time of each case to reach 90 °.

Condition	Time to reach 90 ° (h)
Low humidity without UV	>100
Low humidity with UV	>100
Medium humidity without UV	>100
Medium humidity with UV	60
High humidity without UV	15
High humidity with UV	15

Since the static contact angles of treated samples did not return to the initial value during the 100 hours for all conditions, an extrapolation model is beneficial to predict hydrophobicity behaviour after 100 hours. To model the rate of hydrophobicity recovery, a non-linear regression model using equation 4.1 is implemented and depicted in Figures 4.3 and 4.4.

$$y = A \times ln(t) + B \qquad (4.1)$$

Where: y is the contact angle in degrees, t is time in hours, A is a constant that controls the rate of growth, and B is an angle value at 1 hour [72].

The log trend line coefficients R^2 for each test condition are shown in Table 4.3. The curves in Figures 4.3 and 4.4 can be divided, based on the rate of change, into unsaturated and saturated regions. In the former, the rate changes very rapidly, while in the latter the curve flattens out. Figure 4.3 illustrates two curves of hydrophobicity recovery rate for the samples treated with and without UV for each humidity condition. It can be observed that the rate of change of the hydrophobicity curves at the same humidity condition was almost similar during the unsaturated region regardless whether the samples are treated with or without UV. During the saturation region, in contrast, the rate of change for the samples treated with UV became relatively higher in comparison to the samples treated without UV. This can indicate that the samples exposed to UV could regain their hydrophobicity earlier than those samples that are not exposed to UV although their recovery rate was similar during the unsaturated region.

Table 4.3: Coefficients of the trend lines.

Condition	A	B	R^2
Low humidity without UV	4.1554	60.373	0.8807
Low humidity with UV	5.2058	55.567	0.8445
Medium humidity without UV	6.0519	61.623	0.9067
Medium humidity with UV	6.8453	59.742	0.907
High humidity without UV	6.2486	67.849	0.877
High humidity with UV	7.4835	62.432	0.8386

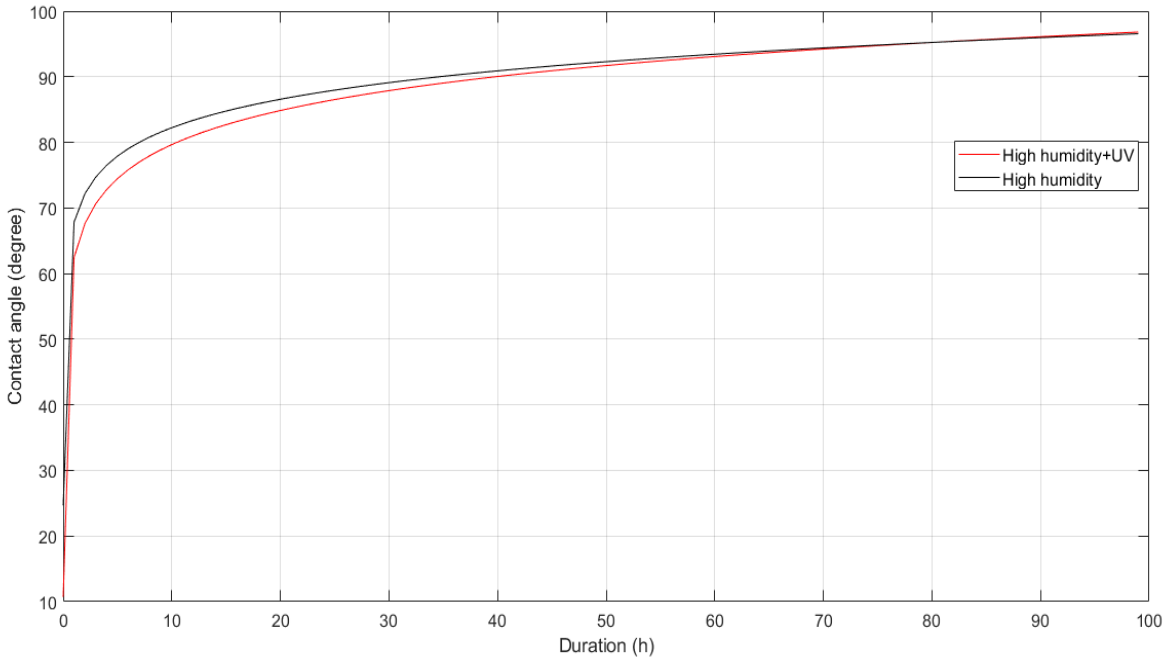
High humidity+UV
High humidity
Contact angle (degree)
Duration (h)
100
90
80
70
60
50
40
30
20
10
0
10
20
30
40
50
60
70
80
90
100

(a)

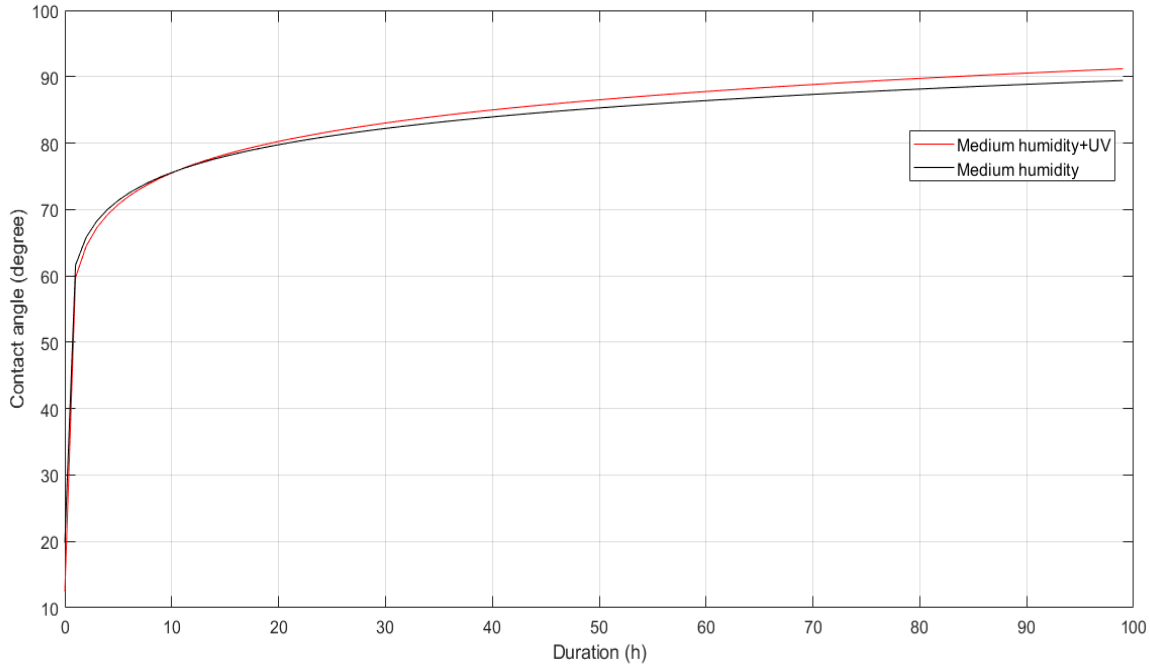
Medium humidity+UV
Medium humidity
Contact angle (degree)
Duration (h)
100
90
80
70
60
50
40
30
20
10
0
10
20
30
40
50
60
70
80
90
100

(b)

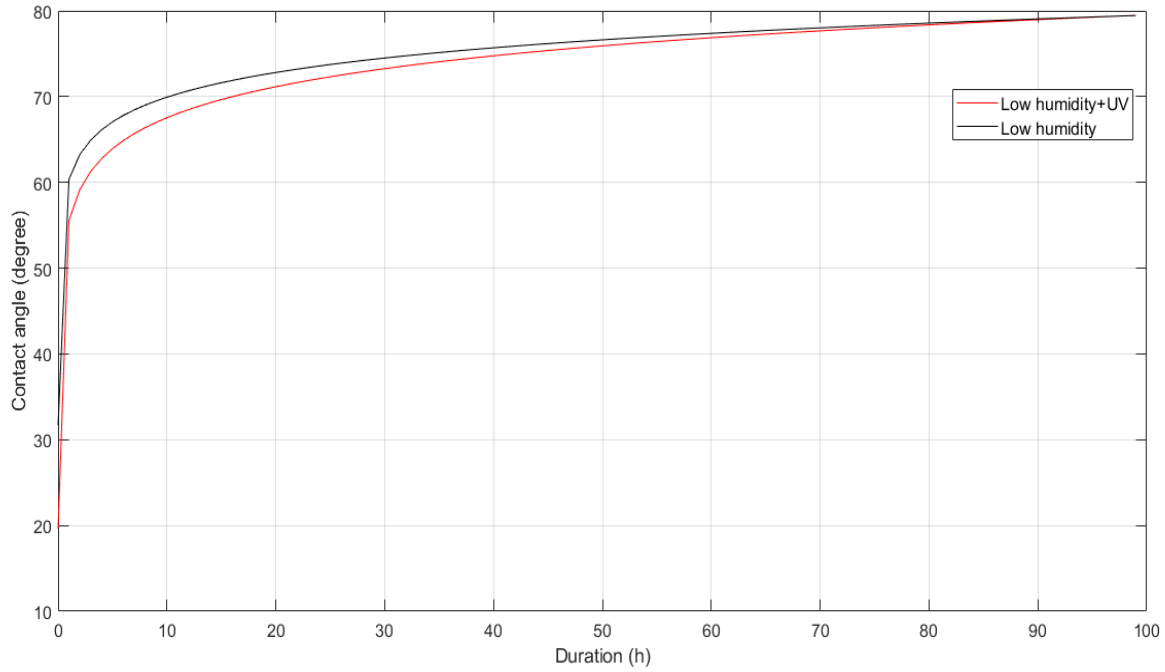

(c)

Figure 4.3. Hydrophobicity recovery rate for SiR after the corona treatment with and without UV radiation under (a) high humidity, (b) medium humidity, and (c) low humidity.

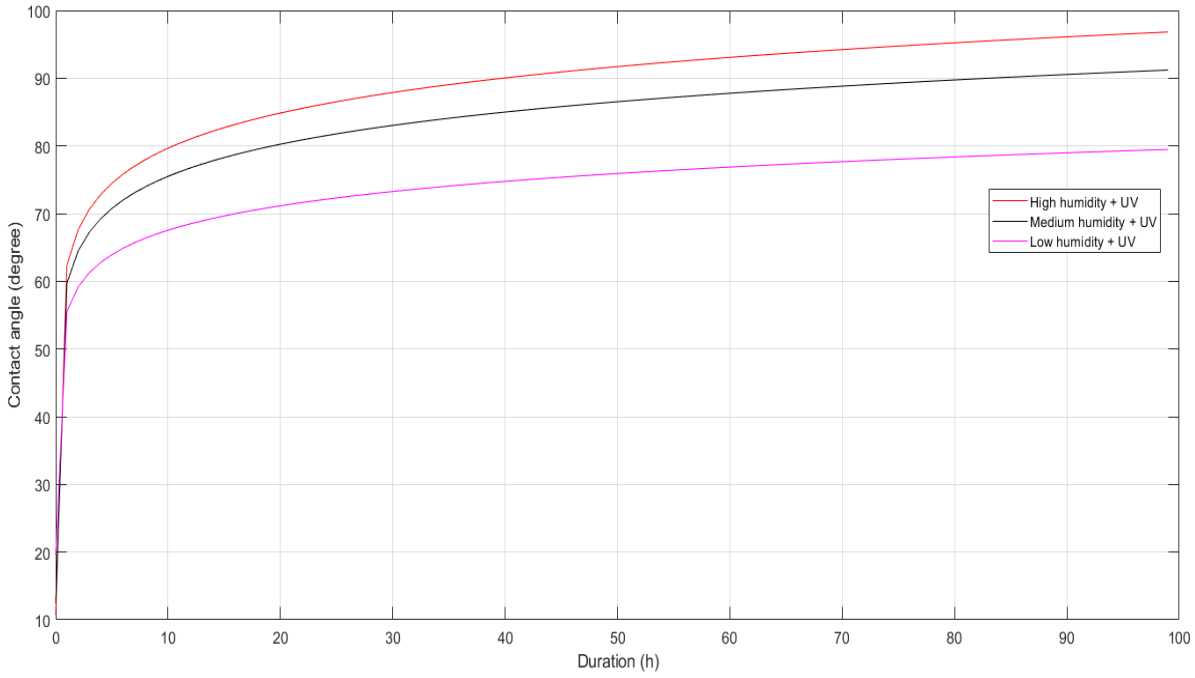

(a)

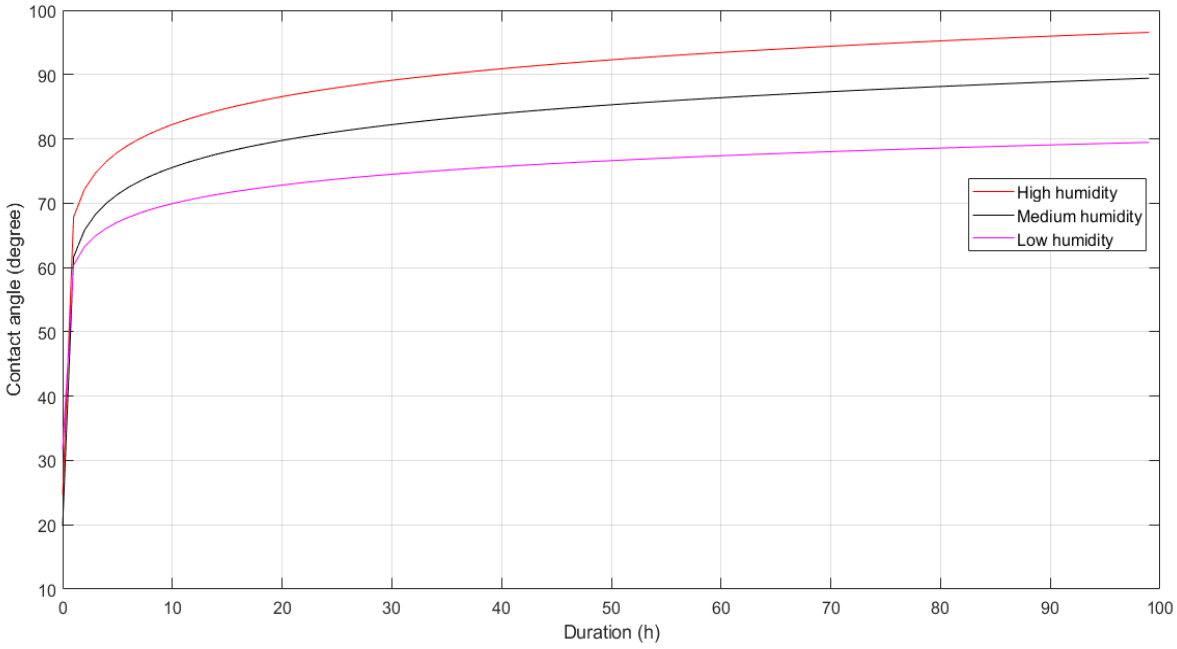

(b)

Figure 4.4. Hydrophobicity recovery rate for SiR after the corona treatment under different humidity levels with (a) UV radiation and (b) without UV radiation.

Moreover, and as represented in Figure 4.4, the rate of change in hydrophobicity recovery curves for the samples treated at the same UV conditions was almost similar during unsaturated region regardless of the humidity level. During the saturated region, on the other hand, the higher the humidity, the larger was the rate of change.

To verify the non-linear regression model, several static contact angles after 100 h were predicted and then compared with the available measured values at their corresponding time, as depicted in Table 4.4. It is evident that the non-linear regression model can be employed for extrapolation to predict the hydrophobicity behaviour.

Overall, among the 6 test conditions, the slowest in full recovery would be low humidity without UV, and the fastest would be UV along with high humidity. The reason behind that could be the impact of tiny physical damage that might have facilitated the migration of the LMW polymer chains. Hence, the surfaces of the treated SiR samples were investigated by SEM with EDX analysis to check the existence of signs of physical damages.

Table 4.4: Comparison between the predicted and the measured static contact angles.

Condition	High humidity without UV			High humidity with UV		
Time (h)	Predicted value (°)	Measured value (°)	Error (%)	Predicted value (°)	Measured value (°)	Error (%)
120	97.6	90	-8.47	98.2	91	-7.91
140	98.8	93	-6.23	99	91	-8.79
160	99.8	91	-9.67	100	91	-9.89
180	100	88	-13.64	101.27	88	-14.77
200	101	88	-13.48	102	89	-14.6
220	101.7	93	-9.35	102.7	91	-12.86
240	102	94	-8.5	103	96	-7.3

SEM images of the SiR samples are presented in Figure 4.5 for unaged, UV aged, both high and low humidity aged samples. Surface of unaged SiR spacemen, as shown in Figure 4.5 (a), is used as a reference for all other aged samples. Based on the SEM image illustrated in Figure 4.5 (b), the sample exposed to UV radiation without other stresses has surface with minimum porosity and roughness which resulted in minimum hydrophobicity loss. After the corona aging test for 24 hours, signs of aging are evident in the SiR samples. These damages occurred in areas that were directly beneath the high voltage electrode. Therefore, these areas suffered to the significant hydrophobicity loss. Figures 4.5 (c-f), depict the appearance of craters on the SiR surfaces treated under low humidity without UV, low humidity with UV, high humidity without UV, and high humidity with UV, albeit no considerable crack was observed in the first three aforementioned cases.

Compared with the sample treated under low humidity with no UV, depicted in Figure 4.5 (d), the craters were more omnidirectionally scattered on the surfaces of the treated samples under low humidity with UV and under high humidity, as represented in Figure 4.5 (c) and (f), respectively. The scattering of the craters in all direction might have worsen the hydrophobicity loss and facilitated the migration of the LMW polymer chains. This indicates that the UV may accelerate the effects of corona on SiR insulators. Also, the higher humidity, the stronger effects of the corona discharges.

On the contrary, surface degradation of the treated SiR material under high humidity with UV including development of tiny cracks was produced by the corona aging test, as illustrated in Figure 4.5 (e). This can explain the rationale behind the exacerbation of the hydrophobicity loss and increase

in the hydrophobicity recovery rate. Overall, the intensity of the corona impacts under high humidity with UV radiation is the highest among the other test conditions.

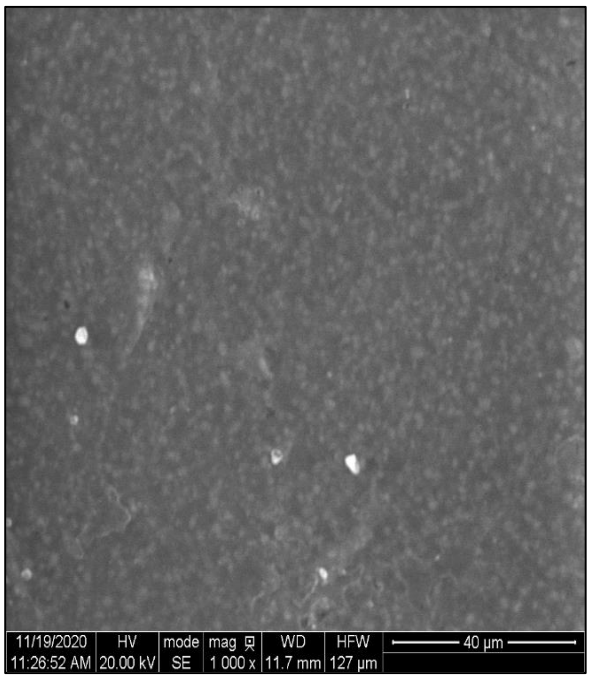

(a)

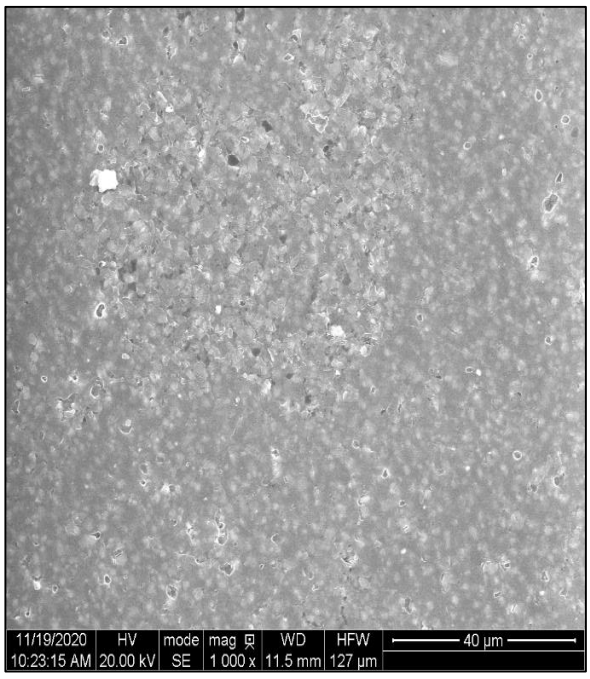

(b)

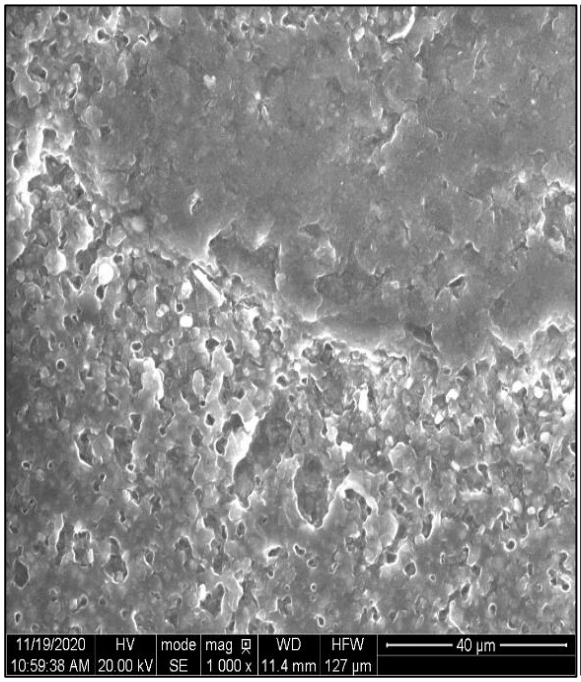

(c)

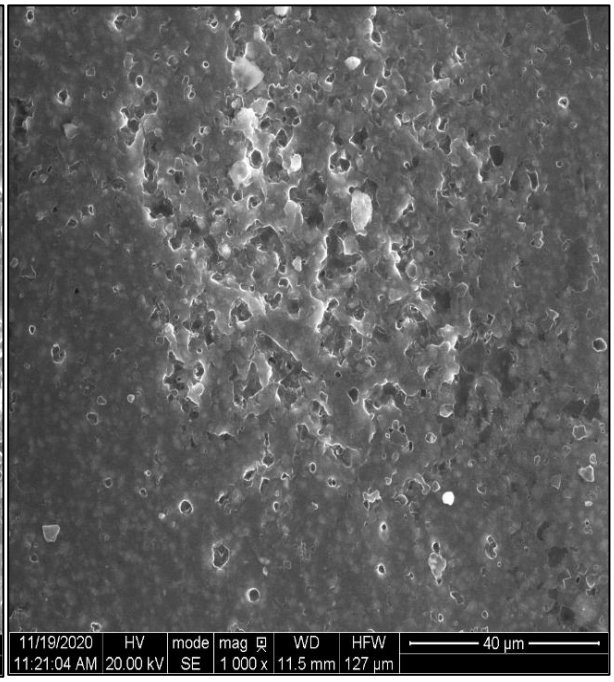

(d)

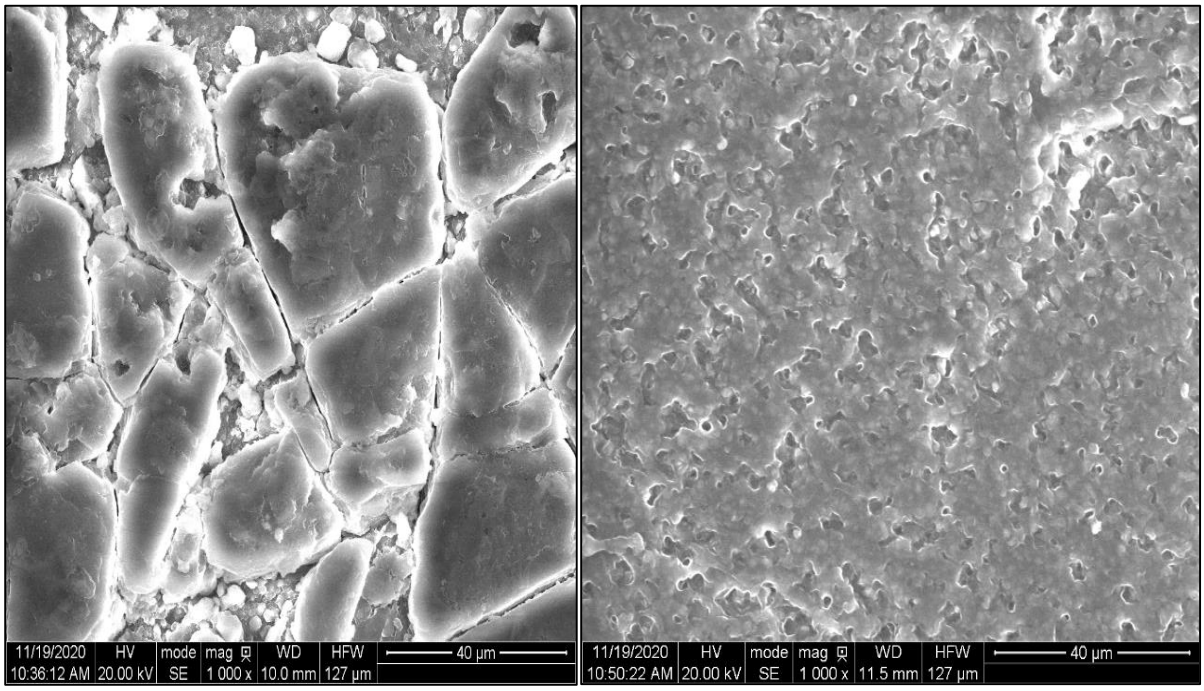

(e) (f)

Figure 4.5 SEM images of SiR samples including: (a) unaged, (b) UV only (c) low humidity with UV, (d) low humidity without UV, (e) high humidity with UV, and (f) high humidity without UV.

The elemental composition of the SiR specimens detected by EDX, presented in Figure 4.6, comprises silicon (Si), aluminum (Al), carbon (C), and oxygen (O). The results of the EDX analysis (in %) are provided in Table 4.5. It was found that Al has decreased drastically on the surface of the samples exposed to corona under UV radiation, regardless of the humidity level. Major decrease in Al signifies the critical reduction in ATH content by the synergistic effect of UV and corona discharges. The attenuation of ATH content will impair the erosion and tracking resistance. Therefore, it was evident that the synergistic effect of UV and corona discharges on the SiR insulator can be momentous.

It was noticeable that there was considerable increase in Si for the samples exposed to corona under UV radiation. This may be caused by the diffusion of LMW polymer chains. No other significant changes in the elements were detected by EDX. This may be attributed to the short duration of the corona test.

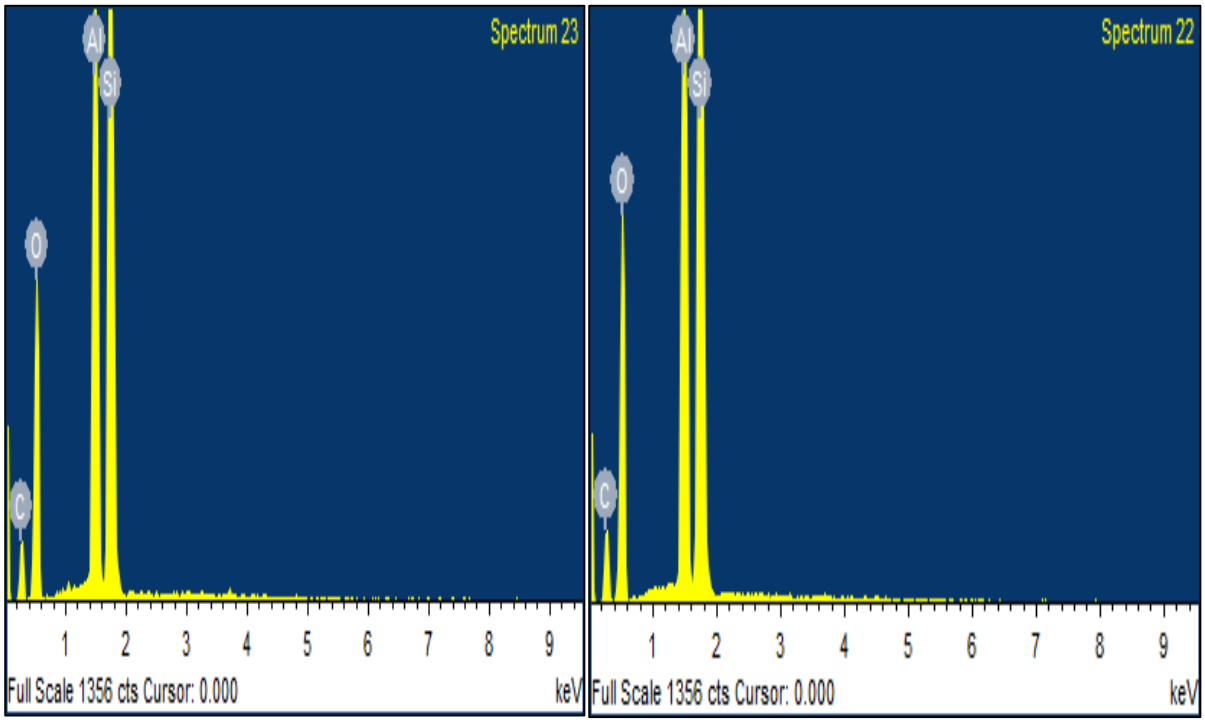
Spectrum 23
Al
Si
O
C
1 2 3 4 5 6 7 8 9
Full Scale 1356 cts Cursor: 0.000
keV
Spectrum 22
Al
Si
O
C
1 2 3 4 5 6 7 8 9
Full Scale 1356 cts Cursor: 0.000
keV

(a) (b)

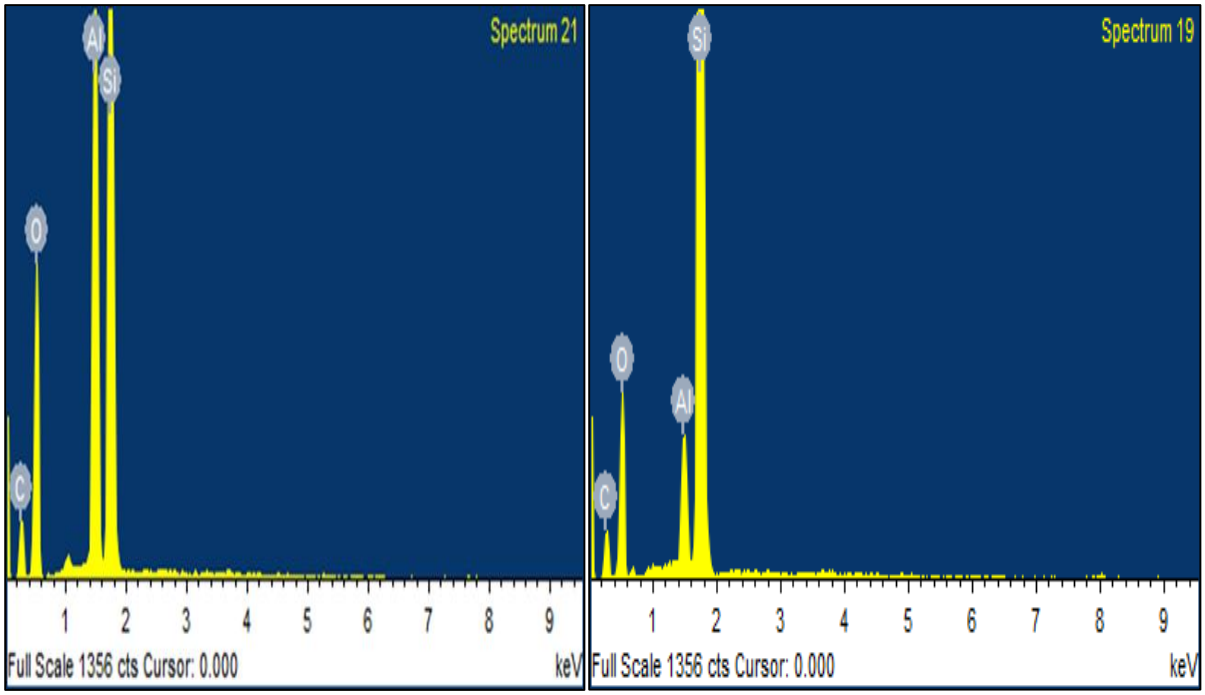
Spectrum 21
Al
Si
O
C
1 2 3 4 5 6 7 8 9
Full Scale 1356 cts Cursor: 0.000
keV
Spectrum 19
Si
O
Al
C
1 2 3 4 5 6 7 8 9
Full Scale 1356 cts Cursor: 0.000
keV

(c) (d)

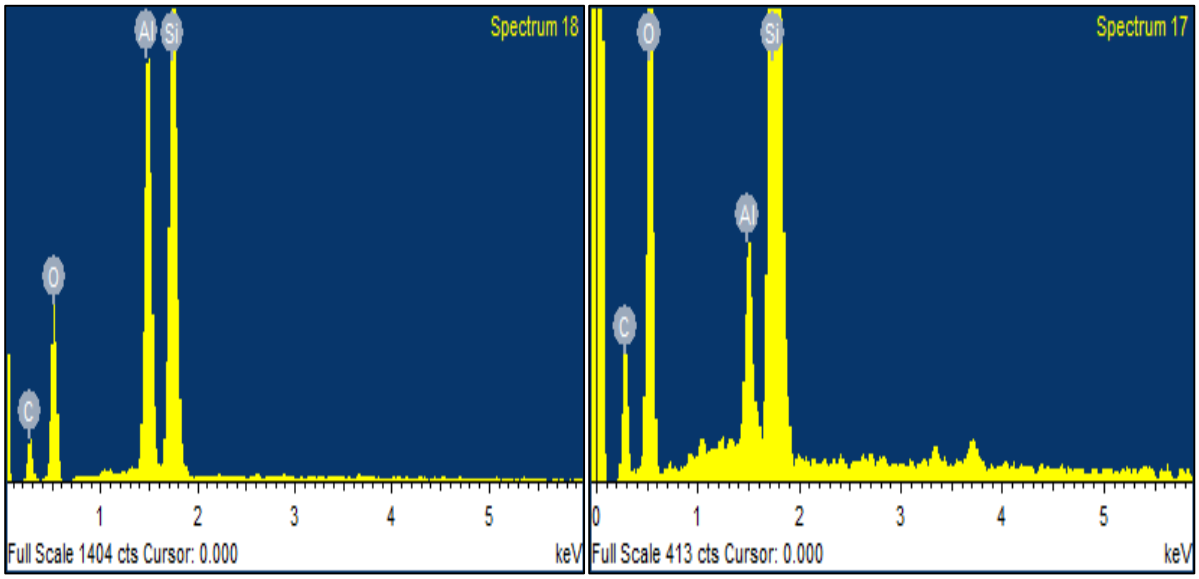

(e) (f)

Figure 4.6. EDX graphs of SiR samples including (a) unaged, (b) aged by UV only, and corona aged under (c) low humidity without UV, (d) low humidity with UV, (e) high humidity without UV, and (f) high humidity with UV.

Table 4.5: Elemental composition for untreated and treated SiR samples.

Conditions	%C	%O	%Al	%Si
Untreated	22.16	41.96	14.81	21.07
Only UV	22.67	43.78	13.52	20.03
Low humidity without UV	22.86	42.41	13.69	21.04
Low humidity with UV	25.59	35.20	3.47	35.73
High humidity without UV	23.89	38.06	14.07	23.98
High humidity with UV	22.48	41.49	1.73	34.30

4.3 Summary

This chapter has discussed the experimental results procured by contact angle measurements, SEM, and EDX analysis to evaluate the performance of the SiR materials with regard to their resistance to corona discharges under acute environmental conditions including UV radiation and high humidity level. The outcomes have shown that both the UV radiation and humidity can accelerate the effects of corona discharges on SiR material.

Chapter 5
Conclusions and Recommendations for Future Work

5.1 Conclusions

This research aimed to investigate the impacts of corona discharges on the silicone rubber (SiR) materials utilized for high voltage outdoor insulators under acute weather conditions such as high humidity level and UV radiation. To achieve this purpose, an aging test setup was designed, and a combination of both high voltage and simulated environmental stresses were proposed. The high voltage stress was applied to test samples using energized needle electrodes at 10 kV to induce the corona discharges on surface of the SiR samples for 24 hours. The gap distance between the surface of samples and the tip of the needle was set at 6 mm. Both the humidity and UV were chosen as the environmental stresses. Both the high voltage and environmental stresses were applied inside a testing chamber. UVA-340 lamps and ultrasonic humidifier were employed to simulate ultraviolet radiation with 1 mW/cm^2 intensity and the humidity condition inside the test chamber, respectively. The corona aging tests were executed under three types of the humidity levels, i.e. high humidity (80 to 90%), medium humidity (65 to 75%), and low humidity (<40%) levels.

Firstly, during the aging experiment, the corona discharges were detected by measuring the high frequency leakage currents. After the aging test, the SiR degradation was assessed through the static contact angle measurements, scanning electron microscopic (SEM) and energy dispersive X-Ray (EDX) analyses. The static contact angle measurements were conducted over 100 hours, following the corona tests to quantify the hydrophobicity loss and recovery. Based on the hydrophobicity loss assessment, it was found that all SiR samples suffered from significant hydrophobicity loss after corona aging test under the different environmental conditions. However, the static contact angle after the aging test was lower when samples were exposed to UV regardless of the humidity level. Consequently, the synergistic impact of UV and corona discharges is evident in the hydrophobicity loss. It was also found that the higher the humidity, the higher variation in the measured contact angles.

Through the hydrophobicity recovery investigation, it has been found that the higher the humidity at the same corona discharges and UV conditions, the faster the hydrophobicity recovery rate for treated samples. On the other hand, it was found that samples treated at the same humidity conditions have similar recovery rate regardless whether the samples were treated with or without UV. Because the

static contact angles of treated samples did not fully regain their hydrophobicity during 100 hours for all conditions, a non-linear regression model was implemented to predict the hydrophobicity behavior after 100 hours. It was predicted that the samples exposed to UV would regain their hydrophobicity earlier than those samples that are not exposed to UV during the saturated region.

Signs of aging in the SiR samples including craters were detected by SEM analysis, especially in areas that were directly under the high voltage electrode. Those signs of aging have resulted in the considerable hydrophobicity loss, and they might have facilitated the migration of the LMW polymer chains leading to achieve faster hydrophobicity recovery. Compared with the sample treated without UV at the same humidity level, the treated samples with UV have more signs of aging. Furthermore, it was worth mentioning that tiny cracks were produced by the corona discharges under high humidity with UV.

Through the EDX analysis, it was revealed that in ATH content on the samples surface was significantly reduced due to the corona exposure under UV radiation leading to reduction in erosion and tracking resistance. Therefore, it can be concluded that the synergistic effect of UV and/ or high humidity level with corona discharges on the SiR insulator can be momentous. Overall, the highest corona impacts were under high humidity with UV condition whilst the lowest were under low humidity without UV condition.

5.2 Contributions

The main contributions of the research presented in this thesis can be found as bellow:

- Investigation of the synergistic impact of UV radiation and corona discharges on SiR insulators was carried out. The UV could exacerbate hydrophobicity loss and increase hydrophobicity recovery rate after the corona exposure. The treated samples with UV had more signs of aging detected by SEM, compared with the samples treated without UV at the same test conditions. The synergistic effects of UV and corona discharges reduced significantly ATH content on the SiR material surface leading to reduction in erosion and tracking resistance.
- Humidity conditions were considered during the corona aging experiments on the SiR materials. The higher the humidity level at the same test conditions, the higher variation in the measured contact angles, the faster the hydrophobicity recovery rate for treated samples, and the further signs of aging detected by SEM.

- After the corona discharges experiments on SiR under different environmental conditions, the SEM results were linked with hydrophobicity behaviour. The further signs of aging, the worse hydrophobicity loss and the faster hydrophobicity recovery rate for treated samples.

5.3 Recommendations for Future Work

The following recommendations for future investigation are highlighted:

- During the hydrophobicity loss evaluation, some cases had relatively high standard deviation. The high standard deviation might be resulted due to the small number of the investigated samples for each case, i.e. three samples per case. Thus, it is suggested to test more samples for each case to reduce the data variability.
- In regard to the hydrophobicity loss, samples tested with corona discharges under different humidity levels without UV exposure did not show any consistent trend. Moreover, no considerable changes in most of elements detected by EDX analysis were found. Those limitations might be attributed to the short duration of the aging test. Hence, a long-term test is recommended for further investigations.
- While SEM and EDX provided good understanding of the physical and chemical changes that happened during the aging process, it is also recommended to conduct further chemical analysis like using FTIR to assess the different chemical bonds in SiR samples after corona aging tests.

Despite the above-mentioned limitations, this research can be an incentive to assess the performance and suitableness of SiR insulators for their applications considering the impact of corona discharges, especially in geographical areas with stringent weather conditions such as UV radiation and humidity.

Bibliography

[1] A. A. Al-Arainy, N. H. Malik and S.M. Al-Ghuwainem , *Fundamentals of Electrical Power Engineering*, Riyadh: King Saud University Press, 2012.

[2] J. Mackevich and M. Shah, "Polymer outdoor insulating materials. Part I: Comparison of porcelain and polymer electrical insulation," *Electrical Insulation Magazine, IEEE,* vol. 13, pp. 5-12, 1997.

[3] CIGRE WG 22.03, "Worldwide service experience with HV composite insulators," *Electra,* No. 191, pp. 27-43, August 2000.

[4] Y. Khan, "Degradation of High Voltage Polymeric Insulators in Arid Desert's Simulated Environmental Conditions," *American J. of Engg. and Applied Sci.*, vol. 2, no. 2, pp. 438-445, 2009.

[5] CIGRE WG D1.14, "Material properties for non-ceramic outdoor insulation: State of the art," *Technical Brochure*, No. 255, 2004.

[6] M. Amin, M. Akbar and M.N. Khan, "Aging Investigations of Polymeric Insulators: Overview and Bibliography," *IEEE Electr. Insul. Mag.*, vol. 23, no. 4, pp. 44-50, 2007.

[7] A. S. Nekeb, "Effect of Some of Climatic Conditions in the Performance of Outdoor HV Silicone Rubber Insulators," PhD dissertation, School of Eng., Cardiff Univ., Cardiff, 2014.

[8] S. İlhan, "Effects of RTV Coating on the Discharge Characteristics of A Suspension Glass Insulator," *Electrica*, vol. 19, no. 2, pp. 173-181 2019.

[9] E. A. Cherney, "Non-Ceramic Insulators - A Simple Design that Requires Careful Analysis," *IEEE Electrical Insulation Magazine*, Vol. 12, No. 3, pp. 7-15,1996.

[10] E. A. Cherney, "50 years in the development of polymer suspension-type insulators," *IEEE. Electr. Insul. Mag.*, vol. 29, no. 3, pp. 18-26, 2013.

[11] E.A. Cherney, “Partial Discharge - Part V: PD in Polymer-type Line Insulators,” *IEEE Electr. Insul. Mag.*, Vol. 7, No. 2, pp. 28-32, 1991.

[12] B. Ma, "Effect of Corona and Ozone Exposure on Properties of Polymeric Materials for High Voltage Outdoor Applications," PhD dissertation, Chalmers Univ. of Technol., Gothenburg, Sweden, 2011.

[13] A. A. Al-Arainy, M. I. Qureshi and N. H. Malik, *Fundamentals of High Voltage Engineering*, Riyadh: King Saud University Press, 2013.

[14] R. Sundararajan , C. Olave, E. Romero and B. Trepanier, "Modified IEC 5000-h multistress aging of 28-kV thermoplastic elastomeric insulators," *IEEE Transactions on Power Delivery*, vol. 22, no. 2, pp. 1079-1085, 2007.

[15] R. A. Ghunem, “A study of the erosion mechanisms of silicone rubber housing composites,” PhD dissertation, ECE, Univ. Waterloo, Waterloo, Canada, 2014.

[16] J. Kim, M. K. Chaudhury and M. J. Owen, "Hydrophobicity Loss and Recovery of Silicone HV Insulation," *IEEE Trans. Dielectrics Elect. Insul.*, vol. 6, pp. 695-702, 1999.

[17] Y. Guo, "Investigation of Silicone Rubber Blends and Their Shape Memory Properties," M.S. thesis, Polym. Eng., Univ. Akron, Akron, OH, USA, 2018.

[18] Q. Wang, X. Liang, W. Bao, T. Jiang and S. Li, "Effect of UV Radiation on Liquid Silicone Rubber," in *2018 IEEE International Conference on High Voltage Engineering and Application (ICHVE)*, ATHENS, Greece, 2018, pp. 1-4, doi: 10.1109/ICHVE.2018.8641864.

[19] A. E. Vlastos and S. M. Gubanski, "Surface structural changes of naturally aged silicone and EPDM composite insulators," *IEEE Trans. on Power Del.*, vol. 6, no. 2, pp. 888-900, April 1991, doi: 10.1109/61.131149.

[20] S. M. Gubanski and A. E. Vlastos, "Wettability of naturally aged silicon and EPDM composite insulators," *IEEE Trans. on Power Del.*, vol. 5, no. 3, pp. 1527-1535, July 1990, doi: 10.1109/61.56997.

[21] Y. Liu *et al*., "Influence of AC corona discharge on contamination layer of composite insulator surface," *Proceedings of the 2015 IEEE Conference on Electrical Insulation and Dielectric Phenomena (CEIDP)*, Ann Arbor, MI, USA, 2015, pp. 197-200.

[22] H. Hillborg, S. Karlsson and U. W. Gedde, "Characterisation of low molar mass siloxanes extracted from crosslinked polydimethylsiloxanes exposed to corona discharges," *Polym.*, vol. 42, no. 21, pp. 8883-8889, Oct 2001.

[23] A. Tzimas, E. D. Silva, S. M. Rowland, B. Boumecid, M. Queen and M. Michel, "Asset management frameworks for outdoor composite insulators," *IEEE Trans. Dielectrics Elect. Insul*, vol. 19, no. 6, pp. 2044-2054, December 2012.

[24] Y.Khan, M.I. Qureshi, N. H. Malik, & A. A Al-Arainy, "Performance of composite insulators in simulated environmental conditions related to central region of Saudi Arabia,"in *2006 Int. Conf. Emerging Technologies*, Peshawar, 2006, pp. 378-384.

[25] M. Amin and M. Ahmed, "Effect of UV Radiation on HTV-Silicon Rubber Insulators with Moisture,"in *2007 IEEE Int. Multitopic Conf.*, Lahore, Pakistan, 2007, pp. 1-5.

[26] M. Tariq Nazir and B. T. Phung, "Ultraviolet weathering resistance performance of micro/nano silica filled silicone rubber composites for outdoor insulation," in *2016 International Conference on Condition Monitoring and Diagnosis*, Xi'an, 2016, pp. 1035-1038.

[27] H. Terrab, A.H. El-hag, A. Bayadi, "Surface analysis of field aged transmission class silicone rubber outdoor insulators" in *2012 Annual Report Conference on Electrical Insulation and Dielectric Phenomena*, Michigan, USA, 2015, pp. 213-216.

[28] Xun Wang, Xidong Liang and Yuanxiang Zhou, "Aging effect of UV radiation on SIR insulators' hydrophobicity property," in *The 17th Annual Meeting of the IEEE Lasers and Electro-Optics Society, 2004. LEOS 2004.*, Boulder, CO, USA, 2004, pp. 241-244.

[29] Y. Khan, A. A. Al-Arainy, N. H. Malik, M. I. Qureshi and A. E. Al-Ammar, “Loss and recovery of hydrophobicity of EPDM insulators in simulated arid desert environment,” in *Asia-Pacific Power and Energy Engineering Conference (APPEEC)*, Chengdu, China, 2010, pp. 1-4.

[30] B. Venkatesulu and M. J. Thomas, “Long–term accelerated weathering of outdoor silicone rubber insulators,” *IEEE Trans. Dielectr. Electr. Insul.*, Vol. 18, No. 2, pp. 418-424, 2011.

[31] A. R. Verma, S. R. B and R. Chakraborty, "Multistress aging studies on polymeric insulators," *IEEE Transactions on Dielectrics and Electrical Insulation*, vol. 25, no. 2, pp. 524-532, April 2018.

[32] W. Bao, X. Liang, Y. Liu, Y. Gao and J. Wang, "Effects of AC and DC corona on the surface properties of silicone rubber: Characterization by contact angle measurements and XPS high resolution scan," *IEEE Transactions on Dielectrics and Electrical Insulation*, vol. 24, no. 5, pp. 2911-2919, Oct. 2017.

[33] R. J. Hollahan and L. G. Carlson, "Hydroxylation of polymethylsiloxane surfaces by oxidizing plasmas," *J. Appl. Polymer Sci.*, Vol. 14, pp. 2499-2508, 1970.

[34] T. G. Gustavsson, S. M. Gubanski, H. Hillborg, S. Karlsson and U. W. Gedde, "Aging of silicone rubber under ac or dc voltages in a coastal environment," *IEEE Transactions on*

Dielectrics and Electrical Insulation, vol. 8, no. 6, pp. 1029-1039, Dec. 2001, doi: 10.1109/94.971462.

[35] H. Hillborg, S. Karlsson, and U. W. Gedde, "Characterisation of low molar mass siloxanes extracted from crosslinked polydimethylsiloxanes exposed to corona discharges," *Polymer*, Vol. 42, pp. 8883-8889, 2001.

[36] B. Ma, S. M. Gubanski and H. Hillborg, " AC and DC corona/ozone-induced ageing of HTV silicone rubber," *IEEE Transactions on Dielectrics and Electrical Insulation*, vol. 18, no. 6, pp. 1984-1994, December 2011.

[37] K. Haji, Y. Zhu, M. Otsubo and C. Honda, "Surface modification of silicone rubber after corona exposure," *Plasma Processes and Polymers*, vol. 4, pp. 1075-1080, 2007, doi: 10.1002/ppap.200732408.

[38] B. Pinnangudi, R. S. Gorur and A. J. Kroese, "Quantification of corona discharges on nonceramic insulators," *IEEE Transactions on Dielectrics and Electrical Insulation*, vol. 12, no. 3, pp. 513-523, June 2005.

[39] A. J. Phillips, D. J. Childs, and H. M. Schneider, "Water drop corona effects on full-scale 500 kV non-ceramic insulators," *IEEE Trans. Power Del.*, vol. 14, no.1, pp. 258-265, 1999.

[40] J. P. Reynders, I. R. Jandrell and S. M. Reynders, "Surface ageing mechanisms and their relationship to service performance of silicone rubber insulation," in *1999 Eleventh Int. Symp. High Voltage Eng.*, London, UK, 1999, pp. 54-58.

[41] M. Kumosa, L. Kumosa, and D. Armentrout, "Causes and potential remedies of brittle fracture failure of composite (nonceramic) insulators," *IEEE Trans. Dielectr. Electr. Insul*., vol. 11, no. 6, pp. 1037-1048, 2004.

[42] M. Kumosa, L. Kumosa, and D. Armentrout, "Failure analyses of nonceramic insulators: part II - the brittle fracture model and failure prevention," *IEEE Electr. Insul. Mag*. vol. 21, no. 4, pp. 28-41, 2005.

[43] A. R. Chughtai, D. M. Smith, L. S. Kumosa, and M. Kumosa, "FTIR analysis of non-ceramic composite insulators," *IEEE Trans. Dielectr. Electr. Insul*., vol. 11,no. 4, pp. 585-596, 2004.

[44] I. Umeda, K. Tanaka, T. Kondo, K. Kondo and Y. Suzuki, "Acid aging of silicone rubber housing for polymer insulators," *Proc. 2008 Int. Symp. on Electr. Insul. Mater.*, Mie, Japan, 2008, pp. 518-521.

[45] B. Ma, J. Andersson and S. M. Gubanski, "Evaluating resistance of polymeric materials for outdoor applications to corona and ozone," *IEEE Trans. Dielectrics Elect. Insul.*, vol. 17, no. 2, pp. 555-565, April 2010.

[46] *Recommended test methods for determining the relative resistance of insulating materials to breakdown by surface discharges*, IEC 60343, 1992.

[47] B. S. Reddy, S. Prasad and M. Rajalingam, "Studies on corona degradation of polymeric insulators," in *2014 6th IEEE Power India Int. Conf.*, Delhi, India, 2014, pp. 1-6.

[48] Y. Zhu, M. Otsubo, C. Honda and S. Tanaka, "Loss and recovery in hydrophobicity of silicone rubber exposed to corona discharge," *Polym. Degradation Stability*, vol. 91, pp. 1448-1454, 2006.

[49] B. S. Reddy and S. P. D, "Effect of coldfog on the corona induced degradation of silicone rubber samples," *IEEE Trans. Dielectrics Elect. Insul.*, vol. 22, no. 3, pp. 1711-1718, June 2015.

[50] J. Zhao, L. Zheng, B. Yan, Y. Wang, L. Mu and L. Lan, "Study on Corona Aging of Room Temperature Vulcanized Silicone Rubber," in *2019 IEEE 3rd Conf. Energy Internet Energy System Integration*, Changsha, China, 2019, pp. 2787-2791.

[51] B. S. Reddy and S. P. D, "Corona degradation of the polymer insulator samples under different fog conditions," *IEEE Trans. Dielectrics Elect. Insul.*, vol. 23, no. 1, pp. 359-367, February 2016.

[52] D. S. Prasad and B. S. Reddy, "Impact of mist and acidic fog on polymer insulator samples exposed to corona discharges," *IEEE Trans. Dielectrics Elect. Insul.*, vol. 23, no. 3, pp. 1546-1554, June 2016.

[53] V. M. Moreno and R. S. Gorur, "AC and DC performance of polymeric housing materials for HV outdoor insulators," *IEEE Trans. Dielectrics Elect. Insul.*, vol. 6, no. 3, pp. 342-350, June 1999.

[54] V. M. Moreno and R. S. Gorur, "Effect of long-term corona on non-ceramic outdoor insulator housing materials," *IEEE Trans. Dielectrics Elect. Insul.*, vol. 8, no. 1, pp. 117-128, Feb 2001.

[55] B. X. Du, Y. Liu and R. L. Wang, " Effects of Corona Discharge on Surface Deterioration of Silicone Rubber Insulator under Reduced Pressures," in *Proc. 2008 Int. Symp. Elect. Insul.*, Mie, Japan, Sep. 7-11, 2008, pp, 271-274.

[56] B. X. Du, H. Xu and Yg Liu, " Effects of Wind Condition on Hydrophobicity Behavior of Silicone Rubber in Corona Discharge Environment," *IEEE Trans. Dielectrics Elect. Insul.*, vol. 23, no. 1, pp. 385-393, 2016.

[57] I. J. S. Lopes, S. H. Jayaram and E. A. Cherney, "A Method for Detecting the Transition from Corona from Water Droplets to Dry-Band Arcing on Silicone Rubber Insulators," *IEEE Trans. Dielectr. Electr. Insul.*, vol. 9, no.6, pp. 964-971, 2002.

[58] L.H. Meyer, E.A. Chemey and S.H. Jayaram, "The role of Inorganic Fillers in Silicone Rubber for Outdoor Insulation - Alumina Tri-hydrate or Silica," *IEEE Electr. Insul. Mag.*, vol. 20, no. 4, pp. 13-21, 2004.

[59] Z. Wang, Z. D. Jia, M. H. Fang, Y. S. Li and Z. C. Guan, "Moisture Absorption, Desorption, and Moisture-induced Electrical Performances of High-temperature Vulcanized Silicone Rubber," *IEEE Trans. Dielectr. Electr. Insul.*, vol. 23, no. 1, pp. 410-417, 2016.

[60] B. Lutz, Z. Guan, L. Wang, F. Zhang and Z. Lü, "Water absorption and water vapor permeation characteristics of HTV silicone rubber material," in *2012 IEEE International Symposium on Electrical Insulation*, San Juan, PR, 2012, pp. 478-482**.**

[61] B. Lutz, L. Cheng, Z. Guan, L. Wang and F. Zhang, " Analysis of a Fractured 500 kV Composite Insulator – Identification of Aging Mechanisms and their Causes, " *IEEE Trans. Dielectr. Electr. Insul.*, vol. 19, no. 5, pp. 1723-1731, 2012.

[62] J. Montesinos, R. S. Gorur, B. Mobasher and D. Kingsbury, "Mechanism of brittle fracture in nonceramic insulators," *IEEE Trans. Dielectr. Electr. Insul*., vol. 9, no. 2, pp. 236-243, 2002**.**

[63] R. Chakraborty and B. S. Reddy, "Studies on high temperature vulcanized silicone rubber insulators under arid climatic aging," *IEEE Trans. Dielectr. Electr. Insul.*, vol. 24, no. 3, pp. 1751-1760, 2017**.**

[64] Z. Li, X. Liang, Y. Zhou, J. Tang, J. Cui and Y. Liu, "Influence of temperature on the hydrophobicity of silicone rubber surfaces," In *Annu. Rep. Conf. Elect. Insul. Dielect. Phenom.*, pp. 679-682, 2004.

[65] J. W. Chang and R. S. Gorur, "Surface recovery of silicone rubber used for HV outdoor insulation," *IEEE Trans. Dielectr. Electr. Insul*., vol. 1, no. 6, pp. 1039-1046, 1994.

[66] R. Chakraborty and S. R. B, "Performance of Silicone Rubber Insulators Under Thermal and Electrical Stress," *IEEE Trans. Industry Appl.*, vol. 53, no. 3, pp. 2446-2454, 2017**.**

[67] A.O. Oladiji, J.O. Borode, B.O. Adewuyi and I.O. Ohijeagbon, "Development of porcelain insulators from locally sourced materials," *USEP: Journal of Research Information in Civil Engineering*, Vol. 7, No. 1, pp. 47-58, 2010**.**

[68] "A Choice of Lamps for the QUV Accelerated Weathering Tester," Q-Lab Corp., Westlake, Ohio, USA, LU-8160, 2019. Accessed: Aug. 20, 2020. [Online]. Available: https://www.q-lab.com/documents/public/d6f438b3-dd28-4126-b3fd-659958759358.pdf

[69] *Composite Insulators for A.C. Overhead Lines with a Nominal Voltage Greater Than 1000 V - Definitions, Test Methods and Acceptance Criteria*", IEC Standard 61109, 1992.

[70] A. Khaled, " ESDD prediction of outdoor polymer insulators," M.S. thesis, Electrical Eng., American Univ. Sharjah, Sharjah, UAE, 2015.

[71] A.F. Stalder, T. Melchior, M. Müller, D. Sage, T. Blu, M. Unser, "Low-Bond Axisymmetric Drop Shape Analysis for Surface Tension and Contact Angle Measurements of Sessile Drops," *Colloids and Surfaces A: Physicochemical and Engineering Aspects*, vol. 364, no. 1-3, pp. 72-81, July 20, 2010.

[72] https://heartbeat.fritz.ai/a-comprehensive-guide-to-logarithmic-regression-d619b202fc8

Appendix A: LabVIEW Code

The following is the illustrations of the LabVIEW code written to control humidity condition in a cyclic manner inside the chamber.

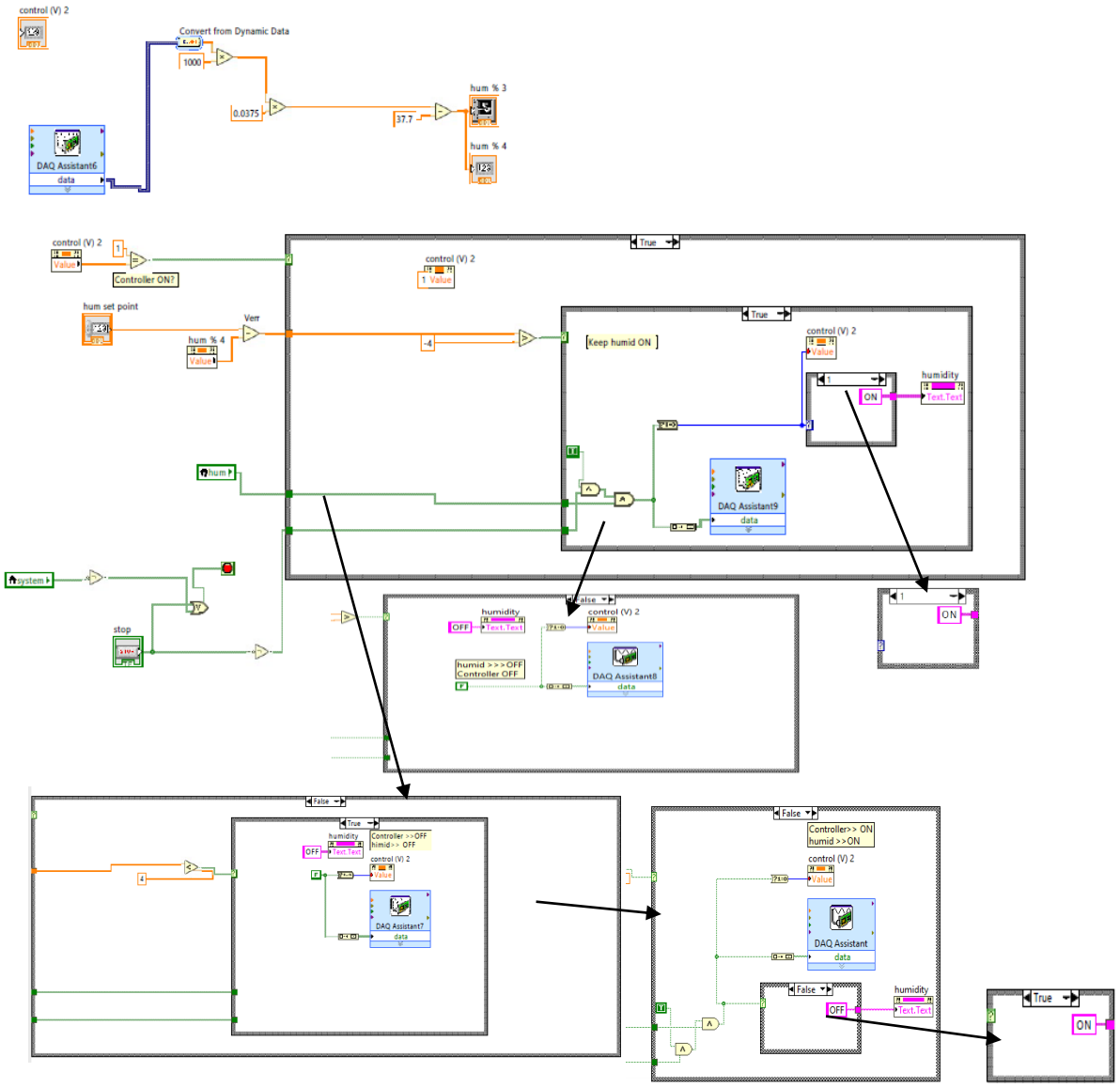

Figure A.1. Humidity Measurement and Control LabVIEW Code.

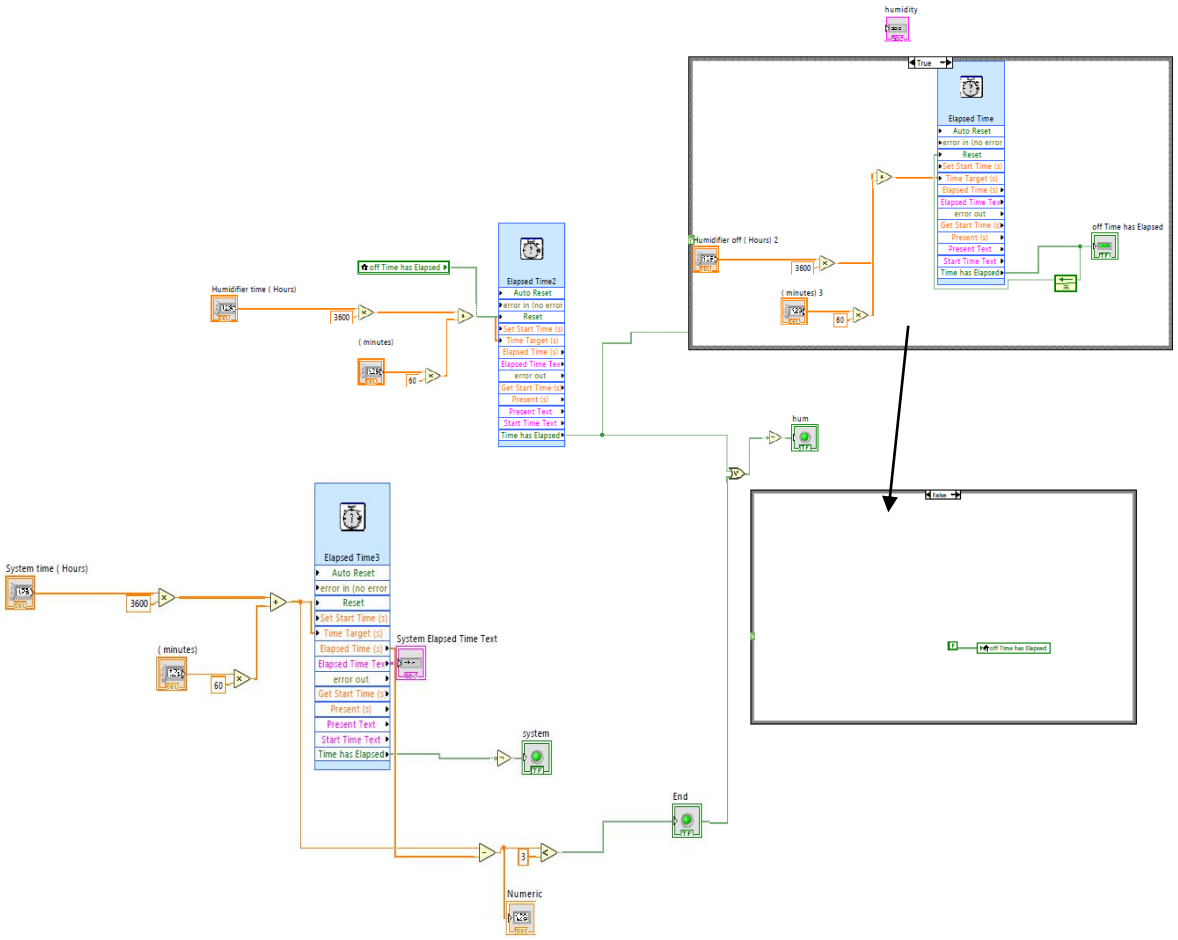

Figure A.2. LabVIEW Code to set cyclic mode for humidifier.

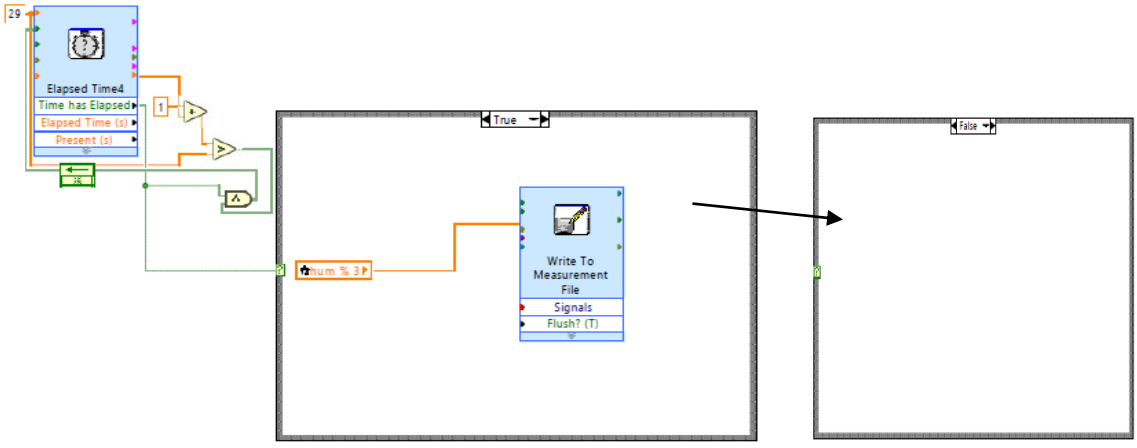

Figure A.3. LabVIEW Code for data recording.